Optimal fine-scale structures in compliance minimization for a shear load

ROBERT V. KOHN
Courant Institute of Mathematical Sciences

AND

BENEDIKT WIRTH
Courant Institute of Mathematical Sciences

Abstract

We return to a classic problem of structural optimization whose solution requires microstructure. It is well-known that perimeter penalization assures the existence of an optimal design. We are interested in the regime where the perimeter penalization is weak, i. e. in the effect of perimeter as a selection mechanism in structural optimization. To explore this topic in a simple yet challenging example, we focus on a 2D elastic shape optimization problem involving the optimal removal of material from a rectangular region loaded in shear. We consider the minimization of a weighted sum of volume, perimeter, and compliance (i. e. the work done by the load), focusing on the behavior as the weight ε of the perimeter term tends to zero. Our main result concerns the scaling of the optimal value with respect to ε. Our analysis combines an upper bound and a lower bound. The upper bound is proved by finding a near-optimal structure, which resembles a rank-two laminate except that the approximate interfaces are replaced by branching constructions. The lower bound, which shows that no other microstructure can be much better, uses arguments based on the Hashin–Shtrikman variational principle. The regime being considered here is particularly difficult to explore numerically, due to the intrinsic nonconvexity of structural optimization and the spatial complexity of the optimal structures. While perimeter has been considered as a selection mechanism in other problems involving microstructure, the example considered here is novel because optimality seems to require the use of two well-separated length scales.

1 Introduction

It is a classic problem to ask what geometry or shape of an elastic body best supports a load while using a minimum amount of material [1]. This question has typically been phrased as the variational task of finding geometries which minimize a weighted sum of volume and compliance (the work done by the load). It has been known for a long time that this problem in many cases requires microstructure, i. e., there are no optimal geometries in the classical sense, but instead an

Communications on Pure and Applied Mathematics, Vol. 000, 0001–0035 (2000)

infinitely fine microstructure is required to achieve the optimal behavior. In particular, so-called laminates (infinitely fine alternating layers of material and void, sometimes arranged in different hierarchies) can always reach that infimum [1]. This situation is somewhat unsatisfactory since infinitely fine microstructures are rather of a theoretical nature and can for instance not be manufactured. As a remedy, a regularizing term can be added to the objective. For strong regularization, there is a broad corresponding literature, which provides the variational analysis as well as numerical implementations using level set formulations [3], phase field approaches [7, 23, 21], multiple materials [7, 23], design-dependent loads [3, 7], nonlinear elasticity [21], and topological regularization [8].

In this article we are instead interested in the case of small regularization, in which very finely structured geometries are optimal. In essence, we ask which structures are selected when perturbing the non-regularized problem by a slight regularization involving the perimeter of the geometry. We approach this question by proving a scaling law for the minimum cost, a nowadays widely used technique in the analysis of variational pattern formation that has already been successfully employed to better understand finely structured configurations in martensitic metals [17, 9], ferromagnets [11], superconductors [10] and other physical situations. In particular, we will prove that the minimum cost for a 2D geometry supporting a shear load on a rectangular boundary (Figure 1.1) scales like $\sqrt{\varepsilon}$ where ε is the weight of the perimeter regularization.

While regularization involving perimeter has been considered in a number of other problems requiring microstructure, most such studies have considered microstructures with a single internal length scale. Our work is different, because the problem we consider requires a microstructure with two well-separated length scales—a so-called rank-two laminate, whose material strips are aligned with the two principal stress directions (at 45° angles with the Euclidean axes). Allaire and Aubry have already observed that this is the only optimal microstructure for a shear load [2] (whereas other loads such as hydrostatic pressure allow various kinds of optimal microstructures). As $\varepsilon \to 0$, our construction of a near-optimal geometry will thus have to approach this microstructure. Our analysis shares some elements with that of [15], which is only natural since the problem considered there also requires two microstructural length scales.

The rest of this introduction discusses the exact form of our objective functional, which is devised to optimize a structure under a fixed shear load, then briefly summarizes results from [16] for the simpler case of compliance optimization under a uniaxial load, and puts forward a brief heuristic argument explaining the observed energy scaling.

1.1 Problem formulation

We consider the minimization of the objective functional

$$\mathrm{J}^{\alpha,\beta,\varepsilon,\mu,F,\ell,L}[\mathscr{O}] = \alpha\mathrm{Comp}^{\mu,F,\ell,L}(\mathscr{O}) + \beta\mathrm{Vol}(\mathscr{O}) + \varepsilon\mathrm{Per}(\mathscr{O})$$

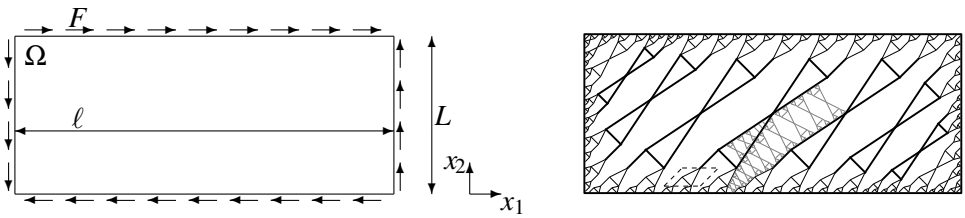

FIGURE 1.1. Left: Load geometry considered in this article. Right: Sketch of a near-optimal geometry as constructed in Section 2. The gray structures are only shown in part of the image.

among all geometries $\mathscr{O} \subset \Omega = [0,\ell] \times [0,L]$, where $\alpha, \beta, \varepsilon > 0$ are positive weights, $\ell, L > 0$ are the geometric parameters, and $\mu > 0, F$ represent a shear modulus and a stress value, respectively (Figure 1.1). $\mathrm{Per}(\mathscr{O})$ denotes the perimeter of the set $\mathscr{O}$, $\mathrm{Vol}(\mathscr{O})$ its volume, and the so-called compliance $\mathrm{Comp}^{\mu,F,\ell,L}(\mathscr{O})$ stands for the mechanical work done by a shear load of magnitude $|F|$ applied at $\partial\Omega$,

$$\mathrm{Comp}^{\mu,F,\ell,L}(\mathscr{O}) = \frac{1}{2}\int_{\partial\Omega} (\bar{\sigma} n)\cdot u \,\mathrm{d}a \quad \text{with } \bar{\sigma} = \left(\begin{smallmatrix} 0 & F \\ F & 0 \end{smallmatrix}\right),$$

where n is the unit outward normal and $u : \mathscr{O} \to \mathbb{R}^2$ is the equilibrium displacement of the loaded structure and thus minimizes the free energy

$$\mathrm{E}^{\mu,F,\ell,L}[u] = \int_{\mathscr{O}} \mu |\varepsilon(u)|^2 \,\mathrm{d}x - \int_{\partial\Omega} (\bar{\sigma} n)\cdot u \,\mathrm{d}a \qquad \text{with } \varepsilon(u) = \tfrac{1}{2}(\nabla u^T + \nabla u).$$

Note that for simplicity we here assumed the structure $\mathscr{O}$ to consist of a homogeneous, isotropic material with zero Poisson's ratio so that the elasticity tensor reduces to the single scalar μ. The existence of minimizing geometries $\mathscr{O}$ for $\varepsilon > 0$ is standard (see e. g. [5, 13, 1, 6]).

The compliance is a measure of the inverse structural stiffness with respect to the imposed load, hence minimization of the compliance yields a structure as rigid as possible. The structure volume and perimeter can for instance be interpreted as material and production costs, respectively.

As already mentioned previously, we are interested in the limit of small perimeter penalization ε. In that limit optimal geometries typically exhibit fine-scale structures which cannot be resolved numerically. Instead we try to provide some understanding by analyzing how the minimum energy scales in ε as $\varepsilon \to 0$. Our analysis involves the construction of a family of near-optimal geometries that give insight into how optimal geometries probably behave. From the viewpoint of variational pattern analysis this problem is very interesting since unlike most others it requires two different fine length scales. Further motivation comes from viewing this variational model as a prototype problem to better understand pattern selection in biological structures, which also often exhibit very fine scales, such as e. g. the spongiosa in bones. Though for instance bone formation is certainly not governed by the variational principle examined in this article, it seems not unreasonable to

assume an evolutionary pressure towards rigid, but light-weight structures. The small perimeter penalization here just limits the possible structural complexity.

It is well-known that the compliance can also be expressed in terms of the equilibrium stress σ rather than the equilibrium displacement u (see e. g. [1]). In detail, by the principle of minimal complementary energy we may write

$$\mathrm{Comp}^{\mu,F,\ell,L}(\mathscr{O}) = \min_{\sigma\in\Sigma_{\mathrm{ad}}^{\mathscr{O}}} \int_{\mathscr{O}} \tfrac{1}{4\mu}|\sigma|^2 \,\mathrm{d}x$$

where the set $\Sigma_{\mathrm{ad}}^{\mathscr{O}}$ of statically admissible stress fields is given by divergence-free symmetric tensor fields satisfying the prescribed stress boundary conditions,

$$\Sigma_{\mathrm{ad}}^{\mathscr{O}} = \{\sigma : \Omega \to \mathbb{R}^{2\times 2}_{\mathrm{sym}} \,|\, \mathrm{div}\sigma = 0 \text{ in } \Omega, \sigma = 0 \text{ in } \Omega\setminus\mathscr{O}, \sigma n = \bar{\sigma} n \text{ on } \partial\Omega\}\,.$$

Finally, a non-dimensionalization yields

$$\mathrm{J}^{\alpha,\beta,\varepsilon,\mu,F,\ell,L}[L\mathscr{O}] = \beta L^2 \mathrm{J}^{1,1,\frac{\varepsilon}{\beta L},\frac{1}{4},F\sqrt{\frac{\alpha}{4\mu\beta}},\frac{\ell}{L},1}[\mathscr{O}] \tag{1.1}$$

so that it suffices to consider the optimization problem of minimizing

$$\mathrm{J}^{\varepsilon,F,\ell}[\mathscr{O}] = \mathrm{Comp}^{F,\ell}(\mathscr{O}) + \mathrm{Vol}(\mathscr{O}) + \varepsilon \mathrm{Per}(\mathscr{O}) \tag{1.2}$$
$$\text{with } \mathrm{Comp}^{F,\ell}(\mathscr{O}) = \min_{\sigma\in\Sigma_{\mathrm{ad}}^{\mathscr{O}}} \int_{\mathscr{O}} |\sigma|^2 \,\mathrm{d}x$$

for $\mathscr{O}\subset\Omega$, where $\Omega = [0,\ell]\times[0,1]$.

For the non-dimensionalized problem, it is known that for $|F| \geq \frac{1}{2}$ the optimal shape $\mathscr{O}$ is the full domain Ω (see e. g. [22]), so the interesting case requires $|F| < \frac{1}{2}$. The purpose of this article is to show the following energy scaling law, the upper and lower bound of which are given in Sections 2 and 3, respectively.

Theorem 1.1 (Optimal energy scaling for shear load)**.** *In the regime $\ell \geq 1$, $\varepsilon < |F| < \frac{1}{2}$, there exist $c, C > 0$ (depending only on ℓ and F) with*

$$c\varepsilon^{\frac{1}{2}} \leq \min_{\mathscr{O}\subset\Omega} \mathrm{J}^{\varepsilon,F,\ell}[\mathscr{O}] - \mathrm{J}_0^{*,F,\ell} \leq C\varepsilon^{\frac{1}{2}}$$

for $\mathrm{J}_0^{*,F,\ell} = 2\ell|F|(2-|F|)$. Here $\Omega = [0,\ell]\times[0,1]$ and $J^{\varepsilon,F,\ell}$ is defined by (1.2)*.*

Above, $\mathrm{J}_0^{*,F,\ell}$ is the infimum of the energy for zero perimeter penalization, $\mathrm{J}_0^{*,F,\ell} = \inf_{\mathscr{O}\subset\Omega} \mathrm{J}^{0,F,\ell}[\mathscr{O}]$. The minimum ceases to exist for $\varepsilon = 0$, and the infimum is realized by a finer and finer sequence of laminates [2]. The infimum value can be obtained as the minimum of the lower semi-continuous envelope of $\mathrm{J}^{0,F,\ell}[\mathscr{O}]$ with respect to weak L^1-convergence of the characteristic function of $\mathscr{O}$, which has long been known [18, 19, 20]. Identifying $\mathscr{O}$ with the set of points where the equilibrium stress is nonzero, we can write

$$\mathrm{J}_0^{*,F,\ell} = \inf_{\sigma\in\Sigma_{\mathrm{ad}}^{\Omega}} \int_\Omega g(\sigma)\,\mathrm{d}x \quad \text{with } g(\sigma) = \begin{cases} 0 & \text{if } \sigma = 0\,, \\ |\sigma|^2 + 1 & \text{else.} \end{cases}$$

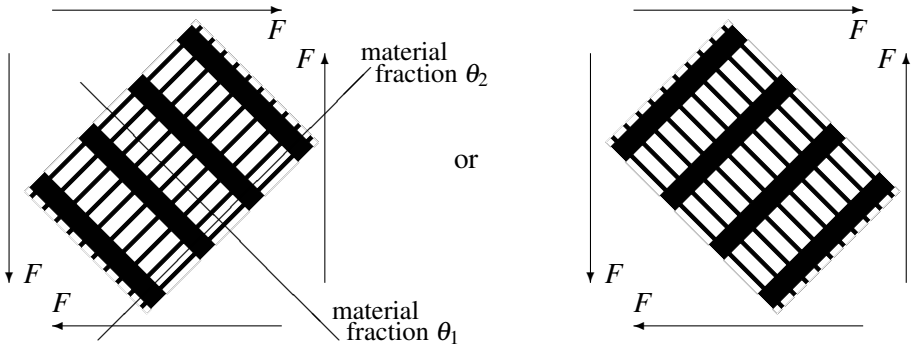

FIGURE 1.2. The optimal microstructure to support a shear load is a two-rank laminate aligned with the two orthogonal principal stress directions. The material strips of the finer scale make up a material fraction $\theta_1 = |F|$ and bear a longitudinal stress of magnitude 1, while the strips of the coarser scale make up a material fraction $\theta_2 = \frac{|F|}{1-|F|}$ and bear a biaxial load of magnitude $1-|F|$ in longitudinal and $|F|$ in transversal direction. The total material fraction is $\theta = (1-\theta_2)\theta_1 + \theta_2 = 2|F|$.

Quasiconvexification of g now yields the lower semi-continuous envelope of the integral [18, 19, 20],

$$\mathrm{J}_0^{*,F,\ell} = \min_{\sigma\in\Sigma_{\mathrm{ad}}^{\Omega}} \int_\Omega \tilde{g}(\sigma)\,\mathrm{d}x \quad \text{with } \tilde{g}(\sigma) = \begin{cases} 2(|\sigma_1|+|\sigma_2|-|\sigma_1\sigma_2|) & \text{if } |\sigma_1|+|\sigma_2|\le 1, \\ 1+\sigma_1^2+\sigma_2^2 & \text{else,} \end{cases}$$

where σ_1 and σ_2 denote the two eigenvalues of the symmetric matrix σ. The minimum is achieved by $\sigma = \bar{\sigma}$. The corresponding microstructure is a rank-two laminate [22] as sketched in Figure 1.2. In our construction of near-optimal geometries for nonzero ε we also have to use two different scales, and we will replace the material strips on both scales by branching constructions.

Remark 1.2. Our proof of the upper bound in fact establishes

$$\min_{\mathscr{O}\subset\Omega} \mathrm{J}^{\varepsilon,F,\ell}[\mathscr{O}] - \mathrm{J}_0^{*,F,\ell} \le \tilde{C}\ell|F|^{\frac{1}{2}}\varepsilon^{\frac{1}{2}}$$

for a constant $\tilde{C}$ independent of ℓ or F under the additional constraint $\varepsilon \le |F|^3$ (i. e., the dependence of C from Theorem 1.1 on ℓ and F is made explicit). It is not clear, though, whether this scaling in ℓ and F is sharp, since our proof of the lower bound does not provide any information on how ℓ and F enter the prefactor in front of $\varepsilon^{\frac{1}{2}}$.

Remark 1.3. Undoing the non-dimensionalization, we obtain a dimensional version of Theorem 1.1: Consider the domain $\Omega = [0,\ell]\times[0,L]$ and the functional defined in (1.1), then in the regime $\ell \ge L$, $2\varepsilon < |F|L\sqrt{\alpha\beta/\mu} < \beta L$, there exist $c, C > 0$ depending only on $\frac{\ell}{L}$ and $F\sqrt{\frac{\alpha}{\mu\beta}}$ with

$$c\big(\tfrac{\ell}{L}, F\sqrt{\tfrac{\alpha}{\mu\beta}}\big)\beta^{\frac{1}{2}}L^{\frac{3}{2}}\varepsilon^{\frac{1}{2}} \le \min_{\mathscr{O}\subset\Omega} \mathrm{J}^{\alpha,\beta,\varepsilon,\mu,F,\ell,L}[\mathscr{O}] - \mathrm{J}_0^{\alpha,\beta,*,\mu,F,\ell,L} \le C\big(\tfrac{\ell}{L}, F\sqrt{\tfrac{\alpha}{\mu\beta}}\big)\beta^{\frac{1}{2}}L^{\frac{3}{2}}\varepsilon^{\frac{1}{2}}$$

for $\mathrm{J}_0^{\alpha,\beta,*,\mu,F,\ell,L} = \ell L|F|\sqrt{\frac{\alpha\beta}{\mu}}(2-|F|\sqrt{\frac{\alpha}{4\mu\beta}})$. The more precise upper bound from the previous remark becomes

$$\min_{\mathscr{O}\subset\Omega} \mathrm{J}^{\alpha,\beta,\varepsilon,\mu,F,\ell,L}[\mathscr{O}] - \mathrm{J}_0^{\alpha,\beta,*,\mu,F,\ell,L} \leq C\ell\sqrt{|F|L\varepsilon}\sqrt[4]{\alpha\beta/\mu}$$

for C independent of the model parameters.

Remark 1.4. We apply a very particular shear load $\bar{\sigma}$ at the domain boundary $\partial\Omega$. We chose this shear load so that the domain Ω has roughly the same extension in both principal stress directions, giving the problem some additional symmetry. If the applied shear stress is slightly rotated to $R(\varphi)\bar{\sigma}R(\varphi)^T$ for some small φ, where $R(\varphi)\in \mathrm{SO}(2)$ denotes rotation by an angle φ, the energy scaling will most likely persist, requiring only slight adaptations of the optimal constructions. However, as the rotation angle φ approaches $\frac{\pi}{4}$, the extension of Ω in one principal stress direction will be much larger, of order ℓ, than in the other direction, where it is of order 1. In that case the horizontally aligned structures will be able to coarsen to a larger degree, thus resulting in a different energy scaling which also involves a power of ℓ. The single construction elements, notably the elementary cells, are expected to stay very similar, though.

1.2 A simpler case: Compliance minimization for a uniaxial load

A shear load represents a biaxial stress state with a compressive and a tensile principal stress in orthogonal directions. A simpler compliance optimization problem is obtained if the shear load on $\partial\Omega$ is replaced by the uniaxial load $\bar{\sigma}_{\mathrm{uni}} n = \left(\begin{smallmatrix}0&0\\0&F\end{smallmatrix}\right) n$, i. e.

$$\min_{\mathscr{O}\subset\Omega} \mathrm{J}_{\mathrm{uni}}^{\varepsilon,F,\ell}[\mathscr{O}] \quad \text{with } \mathrm{J}_{\mathrm{uni}}^{\varepsilon,F,\ell}[\mathscr{O}] = \min_{\sigma\in\Sigma_{\mathrm{ad,uni}}^{\mathscr{O}}} \int_{\mathscr{O}} |\sigma|^2 \,\mathrm{d}x + \mathrm{Vol}(\mathscr{O}) + \varepsilon \mathrm{Per}(\mathscr{O}),$$

where $\Sigma_{\mathrm{ad,uni}}^{\mathscr{O}} = \{\sigma:\Omega\to\mathbb{R}^{2\times 2}_{\mathrm{sym}} \,|\, \mathrm{div}\sigma = 0 \text{ in } \Omega, \sigma = 0 \text{ in } \Omega\setminus\mathscr{O}, \sigma n = \bar{\sigma}_{\mathrm{uni}} n \text{ on } \partial\Omega\}$. The energy scaling law for this functional is determined in [16].

Theorem 1.5 (Optimal energy scaling for uniaxial normal load)**.** *In the regime* $|F|\leq \frac{1}{2}$, $\varepsilon \leq \min(\ell^3|F|, |F|^4)$*, there exist* $c, C > 0$ *(independent of* ℓ *and* F*) with*

$$c\ell|F|^{\frac{1}{3}}\varepsilon^{\frac{2}{3}} \leq \min_{\mathscr{O}\subset\Omega} \mathrm{J}_{\mathrm{uni}}^{\varepsilon,F,\ell}[\mathscr{O}] - \mathrm{J}_{0,\mathrm{uni}}^{*,F,\ell} \leq C\ell|F|^{\frac{1}{3}}\varepsilon^{\frac{2}{3}}$$

for $\mathrm{J}_{0,\mathrm{uni}}^{*,F,\ell} = 2\ell|F|$.

The successful construction is given by a truss-like structure which refines from the center to the boundary via branching as illustrated in Figure 1.3. Each level consists of an array of unit cells with a triangular structure inside, where the unit cell width w halves from level to level and the unit cell height scales like $w^{3/2}$. We will employ such a construction as a structural element in the proof of the upper

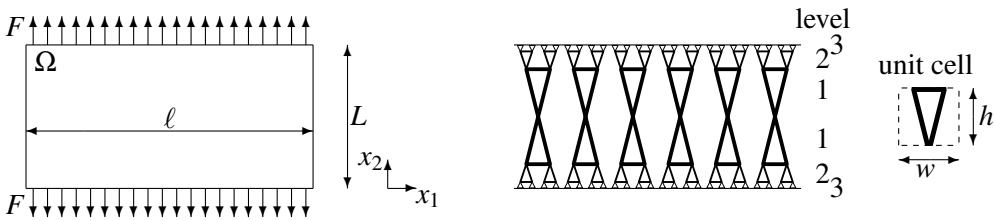

FIGURE 1.3. Left: Load geometry for Theorem 1.5 (uniaxial load) with a uniform normal tension F at the top and bottom. The optimal design $\mathscr{O}$ is sought inside Ω. Right: Sketch of optimal construction (here with three branching levels), which is composed of several unit cells.

bound for the shear load case. We will need a version with $L \neq 1$, which is given by

$$c\ell L^{\frac{1}{3}}|F|^{\frac{1}{3}}\varepsilon^{\frac{2}{3}} \leq \min_{\mathscr{O}\subset\Omega} \mathrm{J}_{\mathrm{uni}}^{\varepsilon,F,\ell,L}[\mathscr{O}] - \mathrm{J}_{0,\mathrm{uni}}^{*,F,\ell,L} \leq C\ell L^{\frac{1}{3}}|F|^{\frac{1}{3}}\varepsilon^{\frac{2}{3}}$$

in the regime $|F| \leq \frac{1}{2}$, $\varepsilon/L \leq \min(\ell^3|F|/L^3, |F|^4)$ and with $\mathrm{J}_{0,\mathrm{uni}}^{*,F,\ell,L} = 2\ell L|F|$.

Let us briefly provide the details of the construction for later usage. We have to specify a geometry together with a stress field and compute its energy. It is convenient to proceed in steps.

Specify unit cell and compute its energy. The employed unit cell of width w and height h is given in Figure 1.4. Its excess energy over the infimum energy for $\varepsilon = 0$ can straightforwardly be computed as [16]

$$\Delta\mathrm{J}_{\mathrm{cell,uni}} = \mathrm{Comp}_{\mathrm{cell,uni}} + \mathrm{Vol}_{\mathrm{cell,uni}} + \varepsilon\mathrm{Per}_{\mathrm{cell,uni}} - 2|F|wh \sim |F|\tfrac{w^3}{h} + \varepsilon(h+w)\,,$$

which becomes $\Delta\mathrm{J}_{\mathrm{cell,uni}}(w) \sim \sqrt{|F|w^3\varepsilon}$ for the optimal $h \sim \sqrt{|F|w^3/\varepsilon}$. Here and in the following, $\sim$ denotes equality up to a constant factor independent of ℓ, L, F, and ε.

Determine coarsest unit cell width and compute total bulk energy. Let us number the levels from 1 (coarsest) to N (finest). Considering only the upper half of the structure (the bottom half is symmetric), the total height $\frac{L}{2}$ has to equal the sum of the heights h_i of the levels, $\frac{L}{2} = \sum_{i=1}^{N} h_i$. Using $h_i = \sqrt{|F|w_i^3/\varepsilon}$ and $w_i = w_1/2^{i-1}$, we arrive at $\frac{L}{2} \sim \sqrt{|F|w_1^3/\varepsilon}$ so that $w_1 \sim \sqrt[3]{L^2\varepsilon/|F|}$. The requirement $w_1 \leq \ell$ then implies the condition $L^2\varepsilon \leq |F|\ell^3$. The total bulk excess energy is

$$\Delta\mathrm{J}_{\mathrm{bulk,uni}} = 2\sum_{i=1}^{N} \frac{\ell}{w_i}\Delta\mathrm{J}_{\mathrm{cell,uni}}(w_i) \sim \ell L^{\frac{1}{3}}|F|^{\frac{1}{3}}\varepsilon^{\frac{2}{3}}\,.$$

Introduce boundary layer. The layering of finer and finer levels has to stop when the unit cell height becomes comparable to the unit cell width, i. e. $h_N \sim w_N$ or equivalently $w_N \sim \varepsilon/|F|$. Between this finest level of unit cells and the top and bottom boundary $\partial\Omega$, respectively, a material layer of thickness $\varepsilon/|F|$ is introduced,

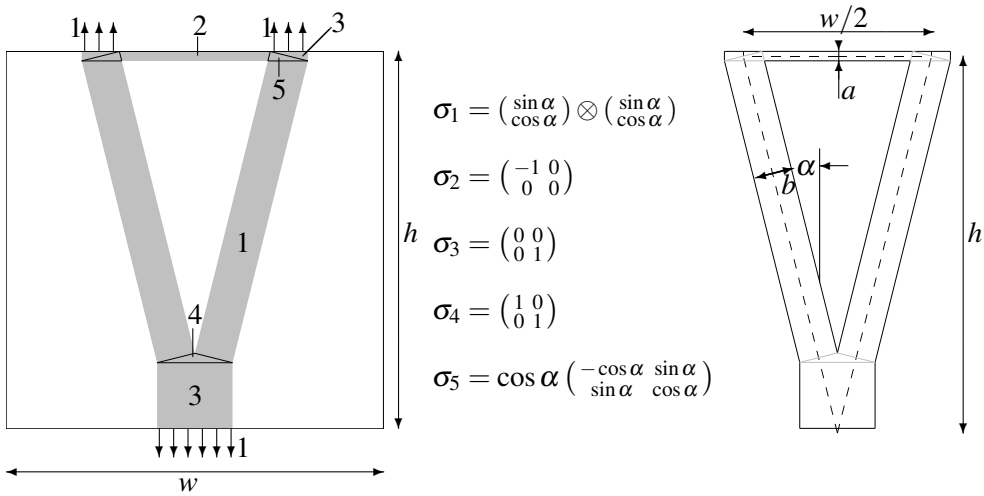

FIGURE 1.4. Sketch of a unit cell for Theorem 1.5; the domains of constant stress are numbered. The right graph serves to indicate the geometric parameters. We take $\tan\alpha = w/4h$, $a = \frac{|F|w}{2}\tan\alpha$, and $b = \frac{|F|w}{2\cos\alpha}$.

which can be shown not to impair the total energy scaling [16]. Furthermore, since $N \geq 1$ or equivalently $w_N \leq w_1$, we obtain the condition $\varepsilon/|F| \leq w_1$ or $\varepsilon/L \leq |F|$.

1.3 A heuristic argument for energy scaling with and without branching

Before proceeding to the details of proving Theorem 1.1, let us provide a brief heuristic argument for the energy scaling with and without branching. For simplicity and as in the previous section, let us call the quantity of interest, $\mathrm{J}^{\varepsilon,F,\ell}[\mathscr{O}] - \mathrm{J}_0^{*,F,\ell}$, the *excess energy* $\Delta\mathrm{J}$ of the geometry $\mathscr{O}$.

Without branching, the geometry will look as in Figure 1.2. Denote by l_1 the length scale or periodicity of the finer struts and by l_2 the period between any two of the coarse struts. The excess energy over the infinitely fine rank-2 laminate has three contributions:

- At $\partial\Omega$, the stresses will deviate from the optimum by an amount of order 1 within a boundary layer of thickness l_2, yielding excess energy $\sim \ell l_2$.
- Likewise, there is a boundary layer of width l_1 where the fine struts meet the coarse bars. Since there are $\sim \ell/l_2$ such boundary layers, the corresponding excess energy contribution is $\sim \ell\frac{l_1}{l_2}$.
- The perimeter contribution comes mostly from the fine struts and thus scales like $\varepsilon\ell/l_1$.

Summarizing, $\Delta\mathrm{J} \sim \ell l_2 + \ell\frac{l_1}{l_2} + \varepsilon\ell/l_1$, which is minimized by $l_1 \sim \varepsilon^{2/3}$ and $l_2 \sim \varepsilon^{1/3}$ to yield $\Delta\mathrm{J} \sim \ell\varepsilon^{1/3}$.

Above, the length scales of the fine and the coarse structures stay spatially constant. This is subobtimal since perimeter energy can be saved by making the length

scales coarser away from $\partial\Omega$. This can for instance be achieved via branching as in Figure 1.1. Let $z = \frac{x_1+x_2}{\sqrt{2}}$ be the coordinate parallel to the coarser layers, and let $l(z)$ be the local length scale of the coarser structure. There are two dominant contributions to the excess energy:

- The effect of the finer-scale structures looks to the coarser-scale structure like an effective surface energy. From the previous section and [16] we know that the corresponding excess energy scales like $\varepsilon^{2/3} l(z)^{1/3} |F|^{1/3}$ per unit length along z. Since there are $\sim \ell/l(z)$ coarse layers, the total contribution of the finer-scale structures is
$$\Delta \mathrm{J}_{\text{fine-scale}} \sim \int_0^1 \varepsilon^{2/3} l(z)^{1/3} |F|^{1/3} \frac{\ell}{l(z)} \,\mathrm{d}z\,.$$
- The excess compliance from branching on the coarser scale behaves like
$$\Delta \mathrm{J}_{\text{coarse-scale}} \sim \ell |F| \int_0^{\frac{1}{2}} (l'(z))^2 \,\mathrm{d}z\,.$$

Both contributions balance when $l'(z)^2 \sim \varepsilon^{2/3} l(z)^{-2/3} |F|^{-2/3}$, i. e. when
$$l(z) \sim \varepsilon^{1/4} |F|^{-1/4} z^{3/4}\,,$$
which produces the expected scaling
$$\Delta \mathrm{J} \sim \Delta \mathrm{J}_{\text{fine-scale}} + \Delta \mathrm{J}_{\text{coarse-scale}} \sim \ell |F|^{1/2} \varepsilon^{1/2}\,.$$

2 Upper bound by two-level branching construction

In this section we will provide a construction which satisfies the upper bound from Theorem 1.1. As mentioned in the introduction, an optimal microstructure for $\varepsilon = 0$ is a rank-two laminate with coarse material strips along one principal stress direction (at a 45° angle with the Euclidean axes) and fine material strips connecting the coarse strips in the orthogonal direction (Figure 1.2). Up to the symmetry of swapping the roles of the two diagonal directions, this rank-two laminate is known to be the unique optimal microstructure for a shear load (as proven in a periodic setting in [2]), and our construction of a near-optimal geometry will thus have to approach this microstructure as $\varepsilon \to 0$. Hence, we will also need two different length scales in the two principal stress directions that both become finer and finer as $\varepsilon \to 0$, but whose scale difference also becomes larger and larger. Also, in order to save perimeter, we will replace the simple material strips by branching constructions similar to the uniaxial case in Section 1.2.

The basic idea of the construction is sketched in Figure 2.1. As a preparation, we first introduce a variation of the construction from Section 1.2 for the uniaxial load case (Section 2.1) as well as an alternative construction for small domain heights (Section 2.2). Those structures will then finally be used inside the construction of near-optimal geometries for the shear load case (Section 2.3). Note that during our construction we will also track the dependence of the resulting

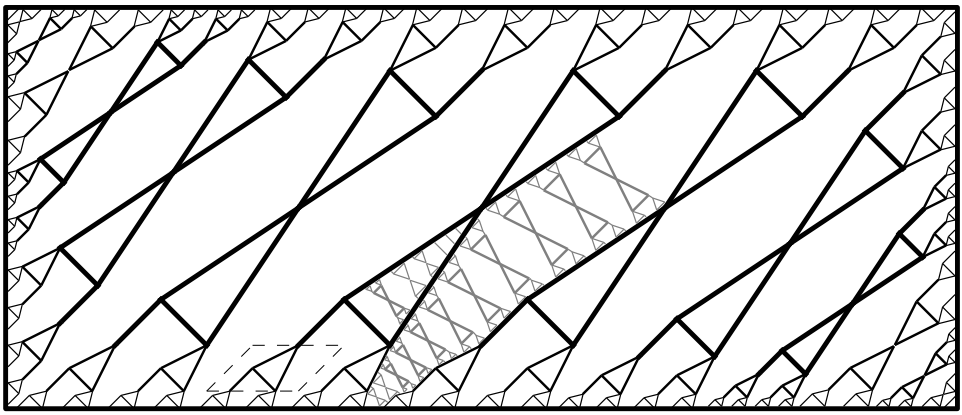

FIGURE 2.1. Sketch of a near-optimal geometry. It exhibits two scales, a coarse one (black) and a finer one in between (gray, not shown everywhere). On the coarser scale the construction is based on several levels that each consist of an array of unit cells (one is framed by a dashed line). The fine scale is based on the construction for a uniaxial load from Section 1.2.

upper energy bound on the parameters ℓ and F, which allows to derive how the constant C in Theorem 1.1 scales in those parameters.

2.1 Construction for a uniaxial load in a non-rectangular domain

Here we consider a variation of the geometry from Section 1.2 in which the upper and lower boundary are not straight, but given as the graph of two Lipschitz-continuous functions $q_1, q_2 : [0,\ell] \to \mathbb{R}$ with Lipschitz constants $L_{q_1}, L_{q_2} \leq 1$ (see Figure 2.2, left). We will use the same notation as in Section 1.2, only keeping in mind that this time Ω is no longer rectangular. We show the following:

Proposition 2.1 (Upper bound for uniaxial load in non-rectangular domain)**.** *Let L_+ and L_- denote the maximum and minimum of $q_1 - q_2$, respectively. In the regime $|F| \leq \frac{1}{2}$, $\varepsilon \leq \min(\ell^3|F|/L_-^2, L_+|F|^4, \frac{1}{16}|F|L_-)$ there exists $C > 0$ with*

$$\min_{\mathscr{O}\subset\Omega} \mathrm{J}_{\mathrm{uni}}^{\varepsilon,F,\ell,q_1,q_2}[\mathscr{O}] - \mathrm{J}_{0,\mathrm{uni}}^{*,F,\ell,q_1,q_2} \leq C\ell L_+^{\frac{1}{3}}|F|^{\frac{1}{3}}\varepsilon^{\frac{2}{3}}$$

for $\mathrm{J}_{0,\mathrm{uni}}^{*,F,\ell,q_1,q_2} = 2|F|\int_0^\ell q_1(x_1) - q_2(x_1)\,\mathrm{d}x_1$.

Proof. We have to provide a geometry and corresponding stress field satisfying the upper bound. We shall use a variation of the construction from Section 1.2. For a better overview, we proceed in steps.

(1) **Segment domain into vertical slabs.** We recursively define the position x_1^n and height H_n of the n^{th} slab's left side as well as the slab width W_n by

$$x_1^1 = 0\,, \quad H_n = q_1(x_1^n) - q_2(x_1^n)\,, \quad W_n = \sqrt[3]{H_n^2\varepsilon/4|F|} \quad x_1^{n+1} = x_1^n + W_n\,,$$

where the width of last slab may be chosen slightly larger so as to fully segment the domain (Figure 2.2, middle). Note that W_n is chosen as the coarsest unit cell width obtained in Section 1.2 for a domain height of $H_n/2$. The reason is that each slab will contain exactly one single tree of a branching construction similar to that of Section 1.2.

(2) **Adapt old branching construction.** Due to the constraints we have $W_n \leq \frac{1}{4}H_n$ so that the domain height $q_1(x_1) - q_2(x_1)$ in the n^{th} slab lies uniformly between $H_n - 2W_n \geq \frac{1}{2}H_n$ and $H_n + 2W_n \leq \frac{3}{2}H_n$. In this slab we now insert one tree of height $\frac{1}{2}H_n$ and width W_n from Section 1.2 (Figure 2.2, right). The tree does not yet reach the upper or lower boundary. This is remedied by introducing additional vertical struts as indicated in Figure 2.2, right. For simplicity we consider just the upper half of the tree, the lower half is treated analogously. Let r_1^0 denote the central root and r_s^m, $s = 1, \dots, 2^m$, the roots of the subtrees on hierarchy level m. We first shift the full tree vertically up until it touches the upper boundary in some point, and then we introduce a vertical strut in between the old and the new root position r_1^0. We then continue with the first level subtrees, that is, we shift up the tree in r_1^1 as well as the tree in r_2^1 until both touch the upper boundary (one of them actually already touched the upper boundary due to the first step) and introduce a vertical strut between their old and their new root positions. This procedure is repeated iteratively over levels $2, 3, \dots$ until every subtree reaches the upper boundary.

(3) **Compute excess energy in the bulk.** Each slab is now tiled by rectangular unit cells (each containing a triangle truss) and rectangles containing only a vertical strut. Here, the vertical strut width is chosen as $w|F|$ so as to achieve a uniform longitudinal stress of magnitude 1 inside. The excess energy $\Delta \mathrm{J}_{\text{cell,uni}}$ of the unit cells is identical to the excess energy computed in Section 1.2, while the excess energy of a vertical strut cell $\mathfrak{C}$ of width w and height h is given by

$$\Delta \mathrm{J}_{\mathfrak{C},\text{uni}} = \mathrm{Comp}_{\mathfrak{C},\text{uni}} + \mathrm{Vol}_{\mathfrak{C},\text{uni}} + \varepsilon \mathrm{Per}_{\mathfrak{C},\text{uni}} - 2|F|wh = 2\varepsilon h$$

and thus is of at most the same order as the excess energy of the attached unit cell (note that the height always satisfies $h \leq w$ and the width $w \geq \frac{\varepsilon}{|F|}$, cf. Section 1.2). Hence, the total bulk excess energy in the n^{th} slab is of the same order as the excess energy of the construction from Section 1.2 in a rectangular domain of width W_n and height $H_n/2$, and the accumulated bulk excess energy is given by

$$\Delta \mathrm{J}_{\text{bulk,uni}} \sim \sum_{n=1}^{\#\text{slabs}} W_n H_n^{\frac{1}{3}} |F|^{\frac{1}{3}} \varepsilon^{\frac{2}{3}} \lesssim \ell L_+^{\frac{1}{3}} |F|^{\frac{1}{3}} \varepsilon^{\frac{2}{3}} .$$

(4) **Add a boundary layer.** From Section 1.2 we know that the finest unit cells at the top and bottom boundary have width $\sim \varepsilon/|F|$. At the top and bottom boundary, we now introduce a material layer of thickness $\varepsilon/|F|$ as shown

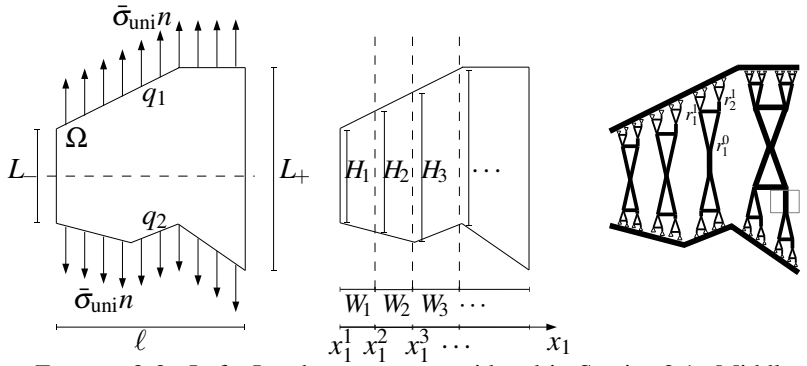

FIGURE 2.2. Left: Load geometry considered in Section 2.1. Middle: Domain decomposition into vertical slabs. Right: Optimal geometry: Each slab is replaced by a truss structure of triangular unit cells; a vertical strut is introduced in between some cells (e. g. in the gray box). Furthermore, a thick material layer is added at the boundary.

in Figure 2.2, right. Its volume scales like $\ell\frac{\varepsilon}{|F|}$, its perimeter like $\ell\varepsilon$, and its compliance is smaller than the volume since the stress never exceeds magnitude 1. The overall energy scaling thus is not impaired.

□

2.2 Construction for a uniaxial load in a wedge

This time consider a wedge-shaped domain as in Figure 2.3, left. Again using the same notation as in Section 1.2, only exchanging the domain Ω by a wedge, we show the following.

Proposition 2.2 (Upper bound for uniaxial load in wedge domain)**.** *For $\ell^2 \geq \varepsilon L$ there exists $C > 0$ with*

$$\min_{\mathscr{O}\subset\Omega} \mathrm{J}_{\text{uni}}^{\varepsilon,F,\ell,L}[\mathscr{O}] - \mathrm{J}_{0,\text{uni}}^{*,F,\ell,L} \leq C\ell\sqrt{\varepsilon L}$$

for $\mathrm{J}_{0,\text{uni}}^{*,F,\ell,L} = 2\ell\frac{L}{2}|F|$.

Proof. We take the following ansatz: We traverse the region between the two load boundaries by N equispaced strips of width $F\ell/N$ and add a boundary layer of thickness $\frac{\ell}{N}$ at the load boundaries (Figure 2.3, right). The volume and compliance of the boundary layer behave like $\ell\frac{\ell}{N}$, the volume and compliance of the strips accumulate to $\mathrm{J}_{0,\text{uni}}^{*,F,\ell,L}$, and the total perimeter behaves like NL. Altogether, the excess energy over $\mathrm{J}_{0,\text{uni}}^{*,F,\ell,L}$ scales like $\ell\frac{\ell}{N} + \varepsilon NL$, which is minimized by $N \sim \frac{\ell}{\sqrt{\varepsilon L}} \geq 1$, yielding the desired bound. □

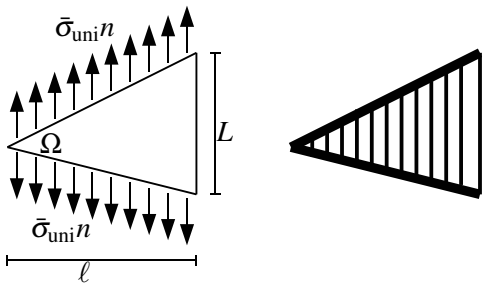

FIGURE 2.3. Left: Load geometry considered in Section 2.2. Right: The proposed geometry consists of vertical struts and a thick material layer at the boundary.

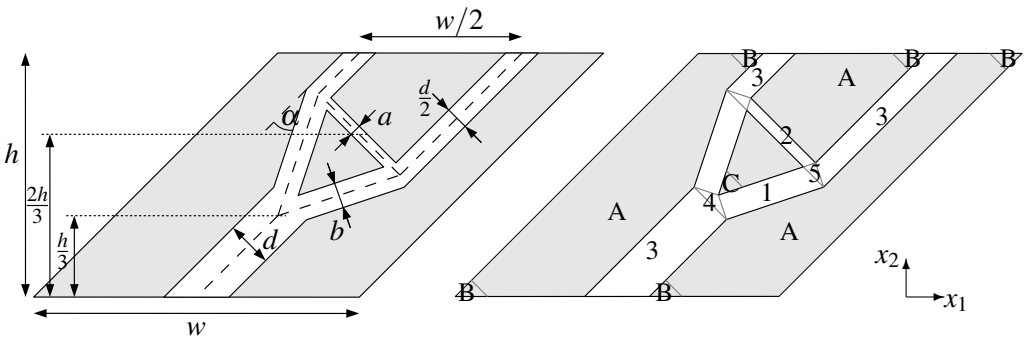

FIGURE 2.4. Sketch of the unit cell for the upper bound in Theorem 1.1. The left sketch indicates the geometric parameters, the right sketch the regions of constant stress. The white regions are full material, the gray regions represent a fine scale branching construction according to Section 2.1 (A) or Section 2.2 (B,C), all rotated counter-clockwise by $\frac{\pi}{4}$. The size of the wedges (B,C) is chosen such that their side parallel to $\binom{-1}{1}$ has length $\sim \frac{\varepsilon}{|F|^4}$.

2.3 A two-scale, unit cell based construction for a shear load

Now we return to the construction of a geometry satisfying the upper bound in Theorem 1.1. The construction is based on the unit cell of width w and height h sketched in Figure 2.4. Ignoring the left and right boundary of Ω for the time being, the construction uses multiple levels, each of which consists of an array of unit cells whose width halves from level to level (Figure 2.1).

As in the construction from Section 1.2, we shall proceed in steps. Without loss of generality let us assume $F > 0$ (changing the sign of F only implies a sign change of the equilibrium stress and thus has no influence on the compliance or the energy scaling).

Specify unit cell and compute its energy. The unit cell is given in Figure 2.4, where the white regions are full material and the gray regions represent a fine scale branching construction according to Section 2.1 (regions A) or Section 2.2 (regions B and C), all rotated counter-clockwise by $\frac{\pi}{4}$. The white material strips correspond

to the coarse strips in the rank-two laminate from Figure 1.2, hence we choose the geometric parameters

$$d = \tfrac{F}{1-F}\tfrac{w}{\sqrt{2}}, \quad \alpha = \tan^{-1}(\tfrac{3w}{8h}), \quad a = \tfrac{d}{2}\tan\alpha, \quad b = \tfrac{d}{2\cos\alpha}.$$

Abbreviating $v_1 = \frac{1}{\sqrt{2}}\binom{1}{1}$, $v_2 = \frac{1}{\sqrt{2}}\binom{-1}{1}$, and $\tilde\sigma = -Fv_2\otimes v_2$ (a uniform compressive stress of magnitude F in direction v_2), the stresses in regions 1 to 5 are then given by

$$\sigma_1 = (1-F)\begin{pmatrix}\cos(\frac{\pi}{4}-\alpha)\\ \sin(\frac{\pi}{4}-\alpha)\end{pmatrix}\otimes\begin{pmatrix}\cos(\frac{\pi}{4}-\alpha)\\ \sin(\frac{\pi}{4}-\alpha)\end{pmatrix}+\tilde\sigma, \quad \sigma_2 = -(1-F)v_2\otimes v_2+\tilde\sigma,$$
$$\sigma_3 = (1-F)v_1\otimes v_1+\tilde\sigma,\ \sigma_4 = (1-F)\mathrm{id}+\tilde\sigma,\ \sigma_5 = (1-F)\cos\alpha\begin{pmatrix}\sin\alpha & \cos\alpha\\ \cos\alpha & -\sin\alpha\end{pmatrix}+\tilde\sigma.$$

The gray regions in Figure 2.4 all exhibit a uniaxial boundary stress of $\tilde\sigma n$ on all of their boundaries so that the constructions from Sections 1.2 to 2.2 can be applied after a rotation by $\frac{\pi}{4}$. Note that while the wedges of type B always have a fixed aspect ratio, the wedges of type C may be very elongated.

A lengthy but straightforward calculation, using Propositions 2.1 and 2.2, now yields the excess energy

$$\begin{aligned}\Delta\mathrm{J}_{\mathrm{cell}} &= \mathrm{Comp}_{\mathrm{cell}}+\mathrm{Vol}_{\mathrm{cell}}+\varepsilon\mathrm{Per}_{\mathrm{cell}}-wh2F(2-F)\\ &\sim hw^{\frac13}F^{\frac13}\varepsilon^{\frac23}+\tfrac{\varepsilon^2}{F^6}+\tfrac{h\varepsilon^2}{wF^6}+(F\tfrac{w^3}{h}+\varepsilon(w+h)),\end{aligned}$$

where the summands correspond to the contributions from the regions A, B, C, and the white region, respectively. Assuming $w \gtrsim \frac{\varepsilon}{F^{19/4}}$ (which we will later ensure), the dominant terms are $hw^{\frac13}F^{\frac13}\varepsilon^{\frac23}+F\frac{w^3}{h}$. Minimizing in h now yields the optimal unit cell height and excess energy,

$$h(w)\sim\sqrt[3]{Fw^4/\varepsilon}, \quad \Delta\mathrm{J}_{\mathrm{cell}}(w)\sim\sqrt[3]{F^2w^5\varepsilon}.$$

Determine coarsest unit cell width and compute total bulk energy. Numbering the refinement levels from 1 (coarsest) to N (finest), the sum of all level heights must equal the total domain height 1, thus

$$1\sim\sum_{i=1}^N h(w_i)=\sum_{i=1}^N h(w_1/2^{i-1})\sim\sqrt[3]{Fw_1^4/\varepsilon}.$$

From this we obtain that the coarsest unit cell width scales like

$$w_1\sim\sqrt[4]{\varepsilon/F}.$$

Finally, the total bulk excess energy is given by

$$\Delta\mathrm{J}_{\mathrm{bulk}}\sim\sum_{i=1}^N\tfrac{\ell}{w_i}\Delta\mathrm{J}_{\mathrm{cell}}(w_i)\sim\tfrac{\ell}{w_1}\Delta\mathrm{J}_{\mathrm{cell}}(w_1)\sim\ell\sqrt{F\varepsilon}.$$

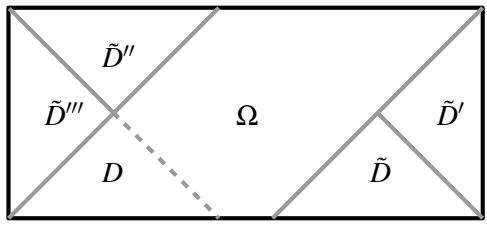

FIGURE 2.5. In the top left and bottom right corner of Ω the construction has to be adapted to the geometry of Ω, using constructions $\tilde{D}, \tilde{D}', \tilde{D}'', \tilde{D}'''$. $\tilde{D}'$ is the reflection of $\tilde{D}$ across the diagonal pointing to the bottom right, and $\tilde{D}''$ and $\tilde{D}'''$ are reflections of $\tilde{D}'$ and $\tilde{D}$ across the other diagonal. The geometry of $\tilde{D}$ will look very similar to a copy of region D.

Introduce boundary layer. The branching has to stop before the unit cell height becomes comparable to the unit cell width. We shall stop a little earlier, as soon as $w_N \sim \frac{\varepsilon}{F^{19/4}}$. The final branching level is connected to $\partial\Omega$ via a material layer of thickness $\frac{\varepsilon}{F^{19/4}}$, introducing an additional volume, compliance, and perimeter term of $\sim \ell \frac{\varepsilon}{F^{19/4}}$. If $\varepsilon \lesssim F^{21/2}$, this is smaller than the bulk energy and thus does not interfere with the overall energy scaling.

Treat left and right end domain ends. At the left and right end of Ω, the coarse level branching trees no longer reach the same height as at the center, since they hit the left or right side of $\partial\Omega$. Using an approach analogous to Section 2.1, in which the left and right end are divided into diagonal slabs, each containing one coarse level branching tree (as in Figure 2.1), it is tedious but straightforward to show that the scaling is not impaired. That this must indeed be so can be understood quite intuitively by noting that the constructions in the domain corners may be viewed as copies (up to slightly stretching or compressing the unit cells to achieve compatibility with the wedge geometry) of a wedge from the bulk construction (Figure 2.5). Thus they do not contribute a larger excess energy than the bulk.

Remark 2.3. In the previous calculation we have shown

$$\min_{\mathscr{O}\subset\Omega} \mathrm{J}^{\varepsilon,F,\ell}[\mathscr{O}] - \mathrm{J}_0^{*,F,\ell} \lesssim \ell\sqrt{|F|\varepsilon}\,,$$

where the feasibility constraints for the construction are $\varepsilon \lesssim |F|^{21/2}$ (so that the boundary layer contribution scales like the bulk energy), $\varepsilon \lesssim |F|\ell^4$ (so that $w_1 \leq \ell$), and $\varepsilon \lesssim |F|^6$ (so that there is at least one layer of unit cells, i. e. $w_1 \geq w_N$). Of course, if F and ℓ are taken as constants which are fixed a priori, this result immediately implies the upper bound in Theorem 1.1.

Remark 2.4. The previous construction is relatively simple to describe, but imposes relatively strong constraints on the relation between ε and F, if one does not consider F as fixed. One can weaken those feasibility constraints by slightly improving

the construction in a way that is no longer based on true unit cells, but looks more like actually shown in Figure 2.1. In detail, the changes are the following.

(1) The coarse-scale branching construction (black in Figure 2.1) stays the same as above, but the fine-scale construction (gray) in between no longer respects the unit cell boundaries. Instead, the gray branching construction extends from one black material strip to the next so that wedges of type B are no longer needed.
(2) In the construction based on Figure 2.4 the gray branching construction of type A refines towards the unit cell boundary as well as towards the white regions, and it is coated on either side with a thin material layer of thickness $\frac{\varepsilon}{F}$ which serves to evenly distribute the stress. In the new refined construction, these material layers are removed so that the finest layer of the branching construction in the gray regions directly touches the white region (in which the stress then distributes evenly over a length scale of $\frac{\varepsilon}{|F|}$). In effect, this changes the constraints of Proposition 2.1, since in its proof the boundary layer contribution to the excess energy no longer scales like $\ell\frac{\varepsilon}{F}$, but instead (due to Corollary A.2 in the appendix) like $\ell\varepsilon|F|\log\frac{1}{|F|}$ so that the bulk energy scaling is not impaired even for $\varepsilon \leq \frac{L_+}{F^2|\log|F||^3}$ (instead of $\varepsilon \leq L_+|F|^4$).
(3) As a result of the previous step, the base length of the wedges of type C can now be chosen as $\frac{\varepsilon}{F}$ instead of $\frac{\varepsilon}{|F|^4}$. Furthermore, also in those wedges the thin boundary material layer from the construction in Proposition 2.2 is removed (so that the material strips across the wedge directly touch the white region in Figure 2.4). This changes the energy scaling in Proposition 2.2: The perimeter term is still εNL, but the excess energy contribution from the boundary layer becomes $\frac{\ell^2}{N}|F|^2\log\frac{1}{|F|}$ (due to Corollary A.2) so that the optimal N now is given by $\ell F\sqrt{\frac{-\log|F|}{\varepsilon L}}$ and the excess energy of a wedge scales like $\ell F\sqrt{\varepsilon L|\log|F||}$.

Summarizing, in essence, the new construction has the same effect as if we had changed the excess energy per unit cell from Figure 2.4 to

$$\Delta \mathrm{J}_{\mathrm{cell}} \sim \tfrac{h}{w}\varepsilon^2\sqrt{\tfrac{|\log|F||}{F}} + hw^{\frac{1}{3}}F^{\frac{1}{3}}\varepsilon^{\frac{2}{3}} + (F\tfrac{w^3}{h} + \varepsilon w + \varepsilon h)\,,$$

where the summands correspond to the contributions from region C, all other gray regions, and the white region, respectively. This time, the condition $w \geq \frac{\varepsilon}{F}$ suffices to achieve $\Delta \mathrm{J}_{\mathrm{cell}}(w) \sim \sqrt[3]{w^5F^2\varepsilon}$. Hence, the branching can now be stopped at $w_N \sim \frac{\varepsilon}{F}$ with a boundary material layer of width $\frac{\varepsilon}{F}$ and energy contribution $\sim \ell\frac{\varepsilon}{F}$, which does not impair the overall scaling as long as $\varepsilon \leq F^3$. The other two constraints ($w_1 \leq \ell$ and $w_1 \geq w_N$) turn into $\varepsilon \lesssim F\ell^4$ and $\varepsilon \lesssim F$.

3 Lower bound by refinement of Hashin–Shtrikman bounds

The Hashin–Shtrikman bounds are bounds on effective elastic moduli of composite materials [14]. In particular they can also be used to bound the compliance of a mixture of void and material under a given macroscopic stress field. A Fourier-based discussion in the context of our 2D shape optimization problem can be found e. g. in [4]. That discussion connects the proof of the bound to the identification of an optimal rank-two laminate. This connection was used in [2] to show that for a shear load as considered here, the Hashin-Shtrikman bound is not achieved by any single-scale periodic composite. We will refine the calculation of [4, 2] to obtain quantitative estimates of

- the cost associated with a misalignment of the geometry with the two principal stress directions (Lemma 3.1),
- the cost associated with a non-optimal material fraction (Lemma 3.1),
- the cost associated with a non-equal distribution of material between the structural parts supporting either of the two principal stresses (Lemma 3.2), and
- the cost associated with an unbalanced spatial distribution of the structural parts supporting either of the two principal stresses (Lemma 3.3).

These estimates will be complemented with

- a Fourier estimate of the geometry perimeter (Lemma 3.5) and
- a Fourier estimate that accounts for the finite size of the geometry and the fact that a uniform shear load has to be fully supported at the domain boundary (Lemma 3.4).

Finally, the non-convexity of the space of possible geometries enters via the simple fact $\chi \cdot \chi = \chi$ for the characteristic function of the optimal geometry. The preceding points will be combined into a proof of the lower bound using an argument by contradiction.

Note that the lower bound for the uniaxial load case from Section 1.2 can be performed in a similar way [16]. However, that case is much simpler since there is only one principal stress direction instead of two so that the estimates concerning the balance between both principal directions are not needed.

3.1 Fourier estimates on compliance, volume, and perimeter

We shall first collect the basic estimates and then combine them into the desired proof. Let $\chi : \Omega \to \{0,1\}$ denote the characteristic function of the optimal geometry $\mathscr{O}$, and let $\theta = \fint_\Omega \chi \, \mathrm{d}x$ denote the corresponding material fraction. We adapt the derivation of the Hashin–Shtrikman bounds from [2] for our purposes. Since we have Neumann rather than periodic boundary conditions for the equilibrium displacement, we will perform the calculation in continuous rather than discrete Fourier space, for which purpose we also require the function

$$\gamma = \chi - \theta \,,$$

extended to $\mathbb{R}^2 \setminus \Omega$ by zero. Note that the L^2-norms of χ and γ can be explicitly computed,

$$\|\chi\|^2_{L^2(\Omega)} = \ell\theta\,, \qquad \|\gamma\|^2_{L^2(\mathbb{R}^2)} = \ell\theta(1-\theta)\,.$$

For a function $f : \mathbb{R}^2 \to \mathbb{R}$ denote by

$$\hat{f}(k) = \int_{\mathbb{R}^2} f(x) e^{-2\pi i k\cdot x}\,\mathrm{d}x$$

its Fourier transform (the inverse transform is given by $\check{g}(k) = \int_{\mathbb{R}^2} g(x) e^{2\pi i k\cdot x}\,\mathrm{d}x$). Finally, for $k \in \mathbb{R}^2$ abbreviate $\bar{k} = \frac{k}{|k|}$ and introduce the set $B = \{v_1, -v_1, v_2, -v_2\}$ for the two principal directions $v_1 = \frac{1}{\sqrt{2}}\left(\begin{smallmatrix}1\\1\end{smallmatrix}\right)$, $v_2 = \frac{1}{\sqrt{2}}\left(\begin{smallmatrix}-1\\1\end{smallmatrix}\right)$ of the imposed shear stress. $\bar{k}^\perp$ shall stand for the counter-clockwise rotation of $\bar{k}$ by $\frac{\pi}{2}$.

We decompose the stress field into the constant $\bar{\sigma}$ and a perturbation η which has zero normal component on $\partial\Omega$ (and which for convenience we extend by zero outside Ω). Introducing

$$\Sigma^0_{\mathrm{ad}} = \{\eta : \mathbb{R}^2 \to \mathbb{R}^{2\times 2}_{\mathrm{sym}} \,|\, \mathrm{div}\eta = 0 \text{ in } \mathbb{R}^2, \eta = 0 \text{ in } \mathbb{R}^2 \setminus \Omega\}\,,$$

we can thus rewrite the structure compliance and volume as follows,

$$\begin{aligned}
&\mathrm{Comp}^{F,\ell}(\mathscr{O}) + \mathrm{Vol}(\mathscr{O}) \qquad (3.1)\\
&= \min_{\substack{\eta\in\Sigma^0_{\mathrm{ad}}\\ (\bar{\sigma}+\eta)(1-\chi)=0 \text{ on } \Omega}} \int_\Omega |\bar{\sigma}+\eta|^2 + \chi\,\mathrm{d}x\\
&\geq \limsup_{K\to 0} \min_{\eta\in\Sigma^0_{\mathrm{ad}}} \int_\Omega |\bar{\sigma}+\eta|^2 + \chi + (1-\chi)K^{-1}|\bar{\sigma}+\eta|^2\,\mathrm{d}x\\
&= \limsup_{K\to 0} \min_{\eta\in\Sigma^0_{\mathrm{ad}}} \int_\Omega |\bar{\sigma}+\eta|^2 + \chi + (1-\chi) \max_{\tau\in\mathbb{R}^{2\times 2}_{\mathrm{sym}}} \left[2(\bar{\sigma}+\eta):\tau - K|\tau|^2\right]\mathrm{d}x\\
&\geq \mathrm{Vol}(\Omega)(|\bar{\sigma}|^2+\theta) + \min_{\eta\in\Sigma^0_{\mathrm{ad}}} \int_\Omega |\eta|^2 + (1-\chi)\left[2(\bar{\sigma}+\eta):\tau\right]\mathrm{d}x
\end{aligned}$$

using Fenchel duality in the second last step and restricting to a fixed, bounded test field τ in the last step. Note that we have also exploited the fact

$$\int_\Omega \eta\,\mathrm{d}x = 0 \quad \text{for all } \eta \in \Sigma^0_{\mathrm{ad}}\,. \qquad (3.2)$$

All estimates for the elastic compliance and material volume are now derived by testing (3.1) with different choices of τ. Note that the test field τ plays a role dual to the stress field, similarly to a strain. However, we are not restricted to choosing τ as the strain of a deformation, and we will later make use of this freedom.

Estimates for material fraction and structure orientation. The simplest choice of τ is a constant. In that case (3.1) can be further simplified to

$$
\begin{aligned}
(3.3)\,&\mathrm{Comp}^{F,\ell}(\mathscr{O})+\mathrm{Vol}(\mathscr{O})\\
&\geq \mathrm{Vol}(\Omega)(|\bar\sigma|^2+2(1-\theta)\bar\sigma:\tau+\theta)+\min_{\eta\in\Sigma^0_{\mathrm{ad}}}\int_{\mathbb{R}^2}|\eta|^2-2\gamma\eta:\tau\,\mathrm{d}x\\
&\geq \ell(|\bar\sigma|^2+2(1-\theta)\bar\sigma:\tau+\theta)+\min_{\hat\eta(k)\in\mathbb{R}^{2\times2}_{\mathrm{sym}}\text{ s.t. }\hat\eta(k)k=0\,\forall k\in\mathbb{R}^2}\int_{\mathbb{R}^2}|\hat\eta|^2-2\bar{\hat\gamma}\hat\eta:\tau\,\mathrm{d}k\\
&=\ell(|\bar\sigma|^2+2(1-\theta)\bar\sigma:\tau+\theta)-\int_{\mathbb{R}^2}|\hat\gamma|^2|\bar k^\perp\cdot\tau\bar k^\perp|^2\,\mathrm{d}k\\
&=\ell(|\bar\sigma|^2+2(1-\theta)\bar\sigma:\tau+\theta-\theta(1-\theta)\max(\tau_1^2,\tau_2^2))\\
&\quad+\max(\tau_1^2,\tau_2^2)\int_{\mathbb{R}^2}|\hat\gamma|^2\left[1-\tfrac{|\bar k^\perp\cdot\tau\bar k^\perp|^2}{\max(\tau_1^2,\tau_2^2)}\right]\mathrm{d}k,
\end{aligned}
$$

where in the second step we used Parseval's identity and in the third step we chose the minimizing $\hat\eta=\hat\gamma(\bar k^\perp\cdot\tau\bar k^\perp)\bar k^\perp\otimes\bar k^\perp$. Here, τ_1 and τ_2 are the eigenvalues of τ. To obtain a tight bound, one can maximize in τ (ignoring the non-negative integral), which leads to an estimate for the elastic excess energy

$$\Delta\mathrm{J}^{F,\ell}_{\mathrm{elast}}(\mathscr{O})=\mathrm{Comp}(\mathscr{O})+\mathrm{Vol}(\mathscr{O})-\mathrm{J}_0^{*,F,\ell}$$

with $\mathrm{J}_0^{*,F,\ell}=2\ell|F|(2-|F|)$.

Lemma 3.1 (Material volume and orientation)**.** *For $B=\{v_1,-v_1,v_2,-v_2\}$ with $v_1=\frac{1}{\sqrt2}\left(\begin{smallmatrix}1\\1\end{smallmatrix}\right)$, $v_2=\frac{1}{\sqrt2}\left(\begin{smallmatrix}-1\\1\end{smallmatrix}\right)$ we have*

$$\Delta\mathrm{J}^{F,\ell}_{\mathrm{elast}}(\mathscr{O})\geq\ell\tfrac{(2|F|-\theta)^2}{\theta}+\tfrac{4F^2}{\theta^2}\int_{\mathbb{R}^2}|\hat\gamma|^2\mathrm{dist}^2(\bar k,B)\,\mathrm{d}k.$$

Proof. Upon inserting the maximizing $\tau=\frac{2\bar\sigma}{\theta}$ into (3.3) and subtracting $\mathrm{J}_0^{*,F,\ell}$ on both sides, we obtain

$$\Delta\mathrm{J}^{F,\ell}_{\mathrm{elast}}(\mathscr{O})\geq\ell\tfrac{(2|F|-\theta)^2}{\theta}+\tfrac{4F^2}{\theta^2}\int_{\mathbb{R}^2}|\hat\gamma|^2\left[1-|\bar k^\perp\cdot\left(\begin{smallmatrix}0&1\\1&0\end{smallmatrix}\right)\bar k^\perp|^2\right]\mathrm{d}k.$$

Now the result follows from $1-|\bar k^\perp\cdot\left(\begin{smallmatrix}0&1\\1&0\end{smallmatrix}\right)\bar k^\perp|^2\geq\mathrm{dist}^2(\bar k,B)$, which can be seen by writing $\bar k=(\cos\varphi,\sin\varphi)^T$ and then noting

$$
\begin{aligned}
1-|\bar k^\perp\cdot\left(\begin{smallmatrix}0&1\\1&0\end{smallmatrix}\right)\bar k^\perp|^2&=1-4\sin^2\varphi\cos^2\varphi=\cos^2(2\varphi)=\sin^2(2\tilde\varphi),\\
\mathrm{dist}^2(\bar k,B)=(1-\cos(\tilde\varphi))^2+\sin^2(\tilde\varphi)&=2(1-\cos(\tilde\varphi))=4\sin^2(\tilde\varphi)\geq\sin^2(2\tilde\varphi)
\end{aligned}
$$

for $\tilde\varphi=(\varphi+\frac{\pi}{2})\bmod\frac{\pi}{2}\in[0,\frac{\pi}{2})$. □

This estimate expresses how much excess energy is paid if the volume fraction θ deviates from $\theta=2|F|$ or if the Fourier transform of the characteristic function has support away from the preferred directions $\pm v_1,\pm v_2$.

Separating the two principal directions. Next let us separate the structural components which mainly support stress in direction v_1 or v_2. Let $s : S^1 \to \{0,1\}$ be the characteristic function on the unit circle of the upper right and lower left quadrant. We define

$$\hat{f}_1(k) = s(\bar{k})\hat{\gamma}(k)\,, \quad \hat{f}_2(k) = (1-s(\bar{k}))\hat{\gamma}(k)$$

and take the inverse Fourier transform to obtain $f_1, f_2 : \mathbb{R}^2 \to \mathbb{R}$. We would like to show that f_1 and f_2 approximately have the same L^2-mass. To this end, we test (3.3) with a constant τ that slightly prefers one direction, i. e., we will perturb τ from Lemma 3.1 by a strain that cannot be supported by the struts encoded in f_2 or f_1, respectively.

Lemma 3.2 (Material distribution between orientations)**.** *For $i = 1,2$ we have*

$$\Delta \mathrm{J}^{F,\ell}_{\mathrm{elast}}(\mathscr{O}) \geq \tfrac{4F^2}{\theta^2 \max(\|f_1\|_{L^2}^2, \|f_2\|_{L^2}^2)} \left(\|f_i\|_{L^2}^2 - \tfrac{\ell\theta(1-\theta)}{2} \right)^2 .$$

Proof. Assume first $\|f_1\|_{L^2}^2 \geq \frac{\ell\theta(1-\theta)}{2}$. This time we use (3.3) with

$$\tau = \frac{2\bar{\sigma}}{\theta} + \frac{4\alpha F}{\theta} v_2 \otimes v_2$$

for some $\alpha \in [0, \frac{1}{3}]$. We obtain

$$\begin{aligned}
\Delta \mathrm{J}^{F,\ell}_{\mathrm{elast}}(\mathscr{O}) &\geq \ell \tfrac{4F^2 - 4|F|\theta + \theta^2 - 8\alpha(1-\theta)F^2}{\theta} + \tfrac{4F^2}{\theta^2} \int_{\mathbb{R}^2} |\hat{\gamma}|^2 \left[1 - |\bar{k}^\perp \cdot \left(\begin{smallmatrix} \alpha & 1-\alpha \\ 1-\alpha & \alpha \end{smallmatrix}\right) \bar{k}^\perp|^2 \right] \mathrm{d}k \\
&\geq \ell \tfrac{(2|F| - \theta)^2 - 8\alpha(1-\theta)F^2}{\theta} + \tfrac{4F^2}{\theta^2} \int_{\mathbb{R}^2} |\hat{f}_1|^2 \left[1 - |\bar{k}^\perp \cdot \left(\begin{smallmatrix} \alpha & 1-\alpha \\ 1-\alpha & \alpha \end{smallmatrix}\right) \bar{k}^\perp|^2 \right] \mathrm{d}k \\
&\geq -\ell \tfrac{8\alpha(1-\theta)F^2}{\theta} + \tfrac{16F^2}{\theta^2} \|\hat{f}_1\|_{L^2}^2 (\alpha - \alpha^2)\,.
\end{aligned}$$

Picking the maximizing $\alpha = \frac{1}{2} - \frac{\ell\theta(1-\theta)}{4\|\hat{f}_1\|_{L^2}^2}$ (which satisfies $0 \leq \alpha \leq \frac{1}{3}$), we obtain

$$\Delta \mathrm{J}^{F,\ell}_{\mathrm{elast}}(\mathscr{O}) \geq \tfrac{4F^2}{\theta^2 \|f_1\|_{L^2}^2} \left(\|f_1\|_{L^2}^2 - \tfrac{\ell\theta(1-\theta)}{2} \right)^2 .$$

In the alternative case $\|f_1\|_{L^2}^2 < \frac{\ell\theta(1-\theta)}{2}$, the relation

$$\|f_1\|_{L^2}^2 + \|f_2\|_{L^2}^2 = \|\hat{f}_1\|_{L^2}^2 + \|\hat{f}_2\|_{L^2}^2 = \|\hat{\gamma}\|_{L^2}^2 = \|\gamma\|_{L^2}^2 = \ell\theta(1-\theta)$$

implies $\|f_2\|_{L^2}^2 \geq \frac{\ell\theta(1-\theta)}{2}$. We repeat the above calculation with $\tau = \frac{2\bar{\sigma}}{\theta} - \frac{4\alpha F}{\theta} v_1 \otimes v_1$ and in the end arrive at $\Delta \mathrm{J}^{F,\ell}_{\mathrm{elast}}(\mathscr{O}) \geq \frac{4F^2}{\theta^2 \|f_2\|_{L^2}^2} \big(\|f_2\|_{L^2}^2 - \frac{\ell\theta(1-\theta)}{2} \big)^2$. Combining both cases yields the desired result. □

So far we have estimates expressing that the structure should be composed of struts aligned with the preferred directions v_1 and v_2, that the struts in both directions should have equal material fraction, and that the total material fraction should be $2|F|$. This does not yet rule out a structure in which the domain Ω is e. g. split into a left and a right half and all the struts in the left are aligned with v_1 while all struts in the right are aligned with v_2. An estimate about the spatial distribution of

the struts in the two directions can be obtained by taking τ piecewise constant. In particular, we will partition Ω into two regions and take the first and second test field from Lemma 3.2 in the first and second region, respectively.

Lemma 3.3 (Spatial distribution of orientations)**.** *Let χ_1, χ_2 be the characteristic functions of Ω_1, Ω_2 with $\Omega_1 \cap \Omega_2 = \emptyset$, $\Omega_1 \cup \Omega_2 = \Omega$, and let $\gamma_i = (\chi - 1)\chi_i - \fint_\Omega (\chi - 1)\chi_i \,\mathrm{d}x$, extended outside Ω by zero. For any $\alpha \in \mathbb{R}$ we have*

$$\Delta \mathrm{J}^{F,\ell}_{\mathrm{elast}}(\mathscr{O}) \geq \ell 4F^2(\tfrac{1}{\theta} - 1)(1 - 2\alpha) \\ - \tfrac{4F^2}{\theta^2} \int_{\mathbb{R}^2} \left| (\overline{\hat{\gamma}_1} + \overline{\hat{\gamma}_2})(1-\alpha)\bar{k}^\perp \cdot \left(\begin{smallmatrix} 0 & 1 \\ 1 & 0 \end{smallmatrix}\right) \bar{k}^\perp + (\overline{\hat{\gamma}_1} - \overline{\hat{\gamma}_2})\alpha \right|^2 \mathrm{d}k \,.$$

Proof. This time we test (3.1) with

$$\tau = \tfrac{2\bar{\sigma}}{\theta} - \tfrac{4\alpha F}{\theta}(\chi_1 \tau_1 + \chi_2 \tau_2) \quad \text{with } \tau_1 = -v_2 \otimes v_2 \,,\ \tau_2 = v_1 \otimes v_1 \text{ and some } \alpha \in \mathbb{R} \,.$$

Subtracting $\mathrm{J}^{*,F,\ell}_0 = 2\ell|F|(2 - |F|)$ on both sides of (3.1), we arrive at

$$\begin{aligned}
\Delta \mathrm{J}^{F,\ell}_{\mathrm{elast}}(\mathscr{O}) &\geq \mathrm{Vol}(\Omega)(4F^2 - 4|F| + \theta) + \min_{\eta \in \Sigma^0_{\mathrm{ad}}} \int_\Omega |\eta|^2 + (1-\chi)\big[2(\bar{\sigma} + \eta) : \tau\big] \,\mathrm{d}x \\
&\geq \ell 4F^2(1 - \tfrac{1}{\theta}) + \min_{\eta \in \Sigma^0_{\mathrm{ad}}} \int_\Omega |\eta|^2 + 2(1-\chi)\bar{\sigma} : \tau \\
&\quad + 2\big[(1-\chi)\chi_1(\tfrac{2\bar{\sigma} - 4\alpha F \tau_1}{\theta}) + (1-\chi)\chi_2(\tfrac{2\bar{\sigma} - 4\alpha F \tau_2}{\theta})\big] : \eta \,\mathrm{d}x \\
&= \ell 4F^2(1 - \tfrac{1}{\theta}) + \ell 8F^2(\tfrac{1}{\theta} - 1) \\
&\quad - \tfrac{4\alpha F}{\theta} \int_\Omega (1-\chi)\left[\chi_2 \left(\begin{smallmatrix} 0 & F \\ F & 0 \end{smallmatrix}\right) : \left(\begin{smallmatrix} 1 & 1 \\ 1 & 1 \end{smallmatrix}\right) - \chi_1 \left(\begin{smallmatrix} 0 & F \\ F & 0 \end{smallmatrix}\right) : \left(\begin{smallmatrix} 1 & -1 \\ -1 & 1 \end{smallmatrix}\right)\right] \mathrm{d}x \\
&\quad + \min_{\eta \in \Sigma^0_{\mathrm{ad}}} \int_\Omega |\eta|^2 + 2\big[(1-\chi)\chi_1(\tfrac{2\bar{\sigma} - 4\alpha F \tau_1}{\theta}) + (1-\chi)\chi_2(\tfrac{2\bar{\sigma} - 4\alpha F \tau_2}{\theta})\big] : \eta \,\mathrm{d}x \\
&= \ell 4F^2(\tfrac{1}{\theta} - 1)(1 - 2\alpha) + \min_{\eta \in \Sigma^0_{\mathrm{ad}}} \int_\Omega |\eta|^2 - 2[\gamma_1(\tfrac{2\bar{\sigma} - 4\alpha F \tau_1}{\theta}) + \gamma_2(\tfrac{2\bar{\sigma} - 4\alpha F \tau_2}{\theta})] : \eta \,\mathrm{d}x \,.
\end{aligned}$$

Passing to Fourier space we obtain

$$\begin{aligned}
\Delta \mathrm{J}^{F,\ell}_{\mathrm{elast}}(\mathscr{O}) &\geq \ell 4F^2(\tfrac{1}{\theta} - 1)(1 - 2\alpha) \\
&\quad + \min_{\hat{\eta}(k) \in \mathbb{R}^{2\times 2}_{\mathrm{sym}} \text{ s.t. } \hat{\eta}(k)k = 0 \,\forall k \in \mathbb{R}^2} \int_{\mathbb{R}^2} |\hat{\eta}|^2 - 2[\overline{\hat{\gamma}_1}(\tfrac{2\bar{\sigma} - 4\alpha F \tau_1}{\theta}) + \overline{\hat{\gamma}_2}(\tfrac{2\bar{\sigma} - 4\alpha F \tau_2}{\theta})] : \hat{\eta} \,\mathrm{d}k \\
&= \ell 4F^2(\tfrac{1}{\theta} - 1)(1 - 2\alpha) - \int_{\mathbb{R}^2} \left| \overline{\hat{\gamma}_1} \bar{k}^\perp \cdot (\tfrac{2\bar{\sigma} - 4\alpha F \tau_1}{\theta}) \bar{k}^\perp + \overline{\hat{\gamma}_2} \bar{k}^\perp \cdot (\tfrac{2\bar{\sigma} - 4\alpha F \tau_2}{\theta}) \bar{k}^\perp \right|^2 \mathrm{d}k \,,
\end{aligned}$$

where we chose the minimizing $\hat{\eta}(k) = \bar{k}^\perp \cdot \big[\hat{\gamma}_1 \tfrac{2\bar{\sigma} - 4\alpha F \tau_1}{\theta} + \hat{\gamma}_2 \tfrac{2\bar{\sigma} - 4\alpha F \tau_2}{\theta}\big] \bar{k}^\perp \bar{k}^\perp \otimes \bar{k}^\perp$. Reordering the different terms we arrive at the desired result. □

We will later employ this result for a very particular partition of the domain. In essence, we will use f_1 and f_2 to identify regions Ω_1 and Ω_2 in which mainly structures along the first and along the second principal direction occur, respectively; Ω_1 and Ω_2 will then serve as the domain partition.

Accounting for compactness of $\mathscr{O}$. Next we employ a continuous Fourier version of a lemma from [11], which captures the fact that the geometry is confined to Ω. For $g:\mathbb{R}\to\mathbb{R}$ with support in the unit interval and a monotonically increasing function $\rho:[0,\infty)\to[0,\infty)$, [11] observes that

$$\begin{aligned}\int_{\mathbb{R}}\rho(|k|)|\hat g(k)|^2\,\mathrm{d}k &\geq \int_{|k|>\frac14}|\hat g(k)|^2\rho(|k|)\,\mathrm{d}k \geq \rho(\tfrac14)\left(\int_{\mathbb{R}}|\hat g|^2\,\mathrm{d}k-\int_{|k|\leq\frac14}|\hat g|^2\,\mathrm{d}k\right)\\ &\geq \rho(\tfrac14)\left(\int_{\mathbb{R}}|\hat g|^2\,\mathrm{d}k-\tfrac12\sup_k|\hat g(k)|^2\right)\geq \tfrac12\rho(\tfrac14)\int_{\mathbb{R}}|\hat g|^2\,\mathrm{d}k\,,\end{aligned}$$

where in the last step we have used $|\hat g|^2\leq\|g\|^2_{L^2([0,1])}=\|\hat g\|^2_{L^2(\mathbb{R})}$ by Hölder's inequality. Essentially, this estimate shows that the Fourier transform of a function with bounded support has a major part of its L^2-mass beyond a frequency k of order 1. In our adapted version, the rôle of g is played by

$$\mathscr{F}_1\gamma(k_1,\cdot)=\int_{\mathbb{R}}\gamma(x_1,\cdot)e^{-2\pi i x_1k_1}\,\mathrm{d}x_1\,,$$

the Fourier transform of γ in the x_1-direction (whose support lies in $x_2\in[0,1]$), and the function ρ is replaced by an approximation of $\mathrm{dist}^2(\bar k,B)$. Our result is the following:

Lemma 3.4 (Compact domain estimate)**.** *For any $b>0$ and $i=1,2$ we have*

$$\Delta\mathrm{J}^{F,\ell}_{\mathrm{elast}}(\mathscr{O})\geq\frac{2F^2}{\theta^2}\,\frac{\int_{\{k:|k\cdot v_i|\leq\frac1b\}}|\hat f_i|^2\,\mathrm{d}k}{1+32\|\gamma\|^4_{L^2}/(b\int_{\{k:|k\cdot v_i|\leq\frac1b\}}|\hat f_i|^2\,\mathrm{d}k)^2}\,.$$

Proof. For any $a,b>0$ we have

$$\begin{aligned}\Delta\mathrm{J}^{F,\ell}_{\mathrm{elast}}(\mathscr{O})&\geq\tfrac{4F^2}{\theta^2}\int_{\mathbb{R}^2}\mathrm{dist}^2(\bar k,B)|\hat\gamma|^2\,\mathrm{d}k\geq\tfrac{4F^2}{\theta^2}\int_{\mathbb{R}^2}\tfrac{(k\cdot v_2)^2}{(k\cdot v_2)^2+(k\cdot v_1)^2}|\hat f_1|^2\,\mathrm{d}k\\ &\geq\tfrac{4F^2}{\theta^2}\tfrac{1}{1+a^2/b^2}\int_{\mathbb{R}}\int_{\{k_2:|k\cdot v_2|\geq\frac1a,|k\cdot v_1|\leq\frac1b\}}|\hat f_1|^2\,\mathrm{d}k_2\,\mathrm{d}k_1\\ &\geq\tfrac{4F^2}{\theta^2}\tfrac{1}{1+a^2/b^2}\int_{\mathbb{R}}\left[\int_{\{k_2:|k\cdot v_1|\leq\frac1b\}}|\hat f_1|^2\,\mathrm{d}k_2-\tfrac{2\sqrt2}{a}\sup_{k_2}|\hat f_1(k_1,k_2)|^2\right]\mathrm{d}k_1\,.\end{aligned}$$

Now we would like to estimate the square-bracketed term by $\int_{\mathbb{R}}|\hat f_1|^2\,\mathrm{d}k_2$ in a similar manner as in the previous estimate from [11]. However, unlike γ, the support of f_1 is not necessarily bounded so that the supremum in the square-bracketed term cannot be bounded above by the L^2-type term. Hence, let us divide the above inequality by

$$C_b=\int_{\{k:|k\cdot v_1|\leq\frac1b\}}|\hat f_1|^2\,\mathrm{d}k\Big/\|\gamma\|^2_{L^2}$$

to obtain

$$\tfrac{\Delta\mathrm{J}^{F,\ell}_{\mathrm{elast}}(\mathscr{O})}{C_b}\geq\tfrac{4F^2}{\theta^2}\tfrac{1}{1+a^2/b^2}\int_{\mathbb{R}}\left[\int_{\mathbb{R}}|\hat\gamma|^2\,\mathrm{d}k_2-\tfrac{2\sqrt2}{C_ba}\sup_{k_2}|\hat f_1(k_1,k_2)|^2\right]\mathrm{d}k_1\,.$$

Choosing $a = \sup_{k_1} \frac{4\sqrt{2}}{C_b} \frac{\sup_{k_2} |\hat{f}_1(k_1,k_2)|^2}{\int_{\mathbb{R}} |\hat{\gamma}|^2 \,\mathrm{d}k_2} \leq \frac{4\sqrt{2}}{C_b} \sup_{k_1} \frac{\sup_{k_2} |\hat{\gamma}(k_1,k_2)|^2}{\int_{\mathbb{R}} |\hat{\gamma}|^2 \,\mathrm{d}k_2} \leq \frac{4\sqrt{2}}{C_b} \sup_{k_1} \frac{\|\mathscr{F}_1\gamma(k_1,\cdot)\|_{L^1}^2}{\|\mathscr{F}_1\gamma(k_1,\cdot)\|_{L^2}^2}$ $\leq \frac{4\sqrt{2}}{C_b}$, where the last step follows from the bounded support of $\mathscr{F}_1\gamma(k_1,\cdot)$, we finally arrive at

$$\Delta \mathrm{J}^{F,\ell}_{\mathrm{elast}}(\mathscr{O}) \geq \frac{2F^2}{\theta^2} \frac{C_b \|\gamma\|_{L^2}^2}{1+32/(bC_b)^2},$$

which after inserting C_b yields the desired inequality for f_1. The analogous calculation can be performed for f_2. □

Intuitively, if b is chosen small, the above estimate basically turns into a bound on $\int_{\{k:|k\cdot v_i|\leq \frac{1}{b}\}} |\hat{f}_i|^2 \,\mathrm{d}k$ of the form $\int_{\{k:|k\cdot v_i|\leq \frac{1}{b}\}} |\hat{f}_i|^2 \,\mathrm{d}k \lesssim \sqrt[3]{\Delta \mathrm{J}^{F,\ell}_{\mathrm{elast}}(\mathscr{O})/b^2}$.

Perimeter estimate. The perimeter can be estimated in Fourier space as in [15, Lemma 4.3, step 2]. We reproduce the brief argument for the sake of completeness.

Lemma 3.5 (Perimeter estimate)**.** *For any $L > 0$ we have*

$$\mathrm{Per}(\mathscr{O}) \geq \frac{1}{L} \int_{\{L|k|\geq 1\}} |\hat{\gamma}|^2 \,\mathrm{d}k.$$

Proof. For any $L > 0$,

$$\begin{aligned}
\mathrm{Per}(\mathscr{O}) &\geq \frac{1}{2\pi L} \int_{\partial B_L(0)} \frac{1}{|c|} \|\gamma - \gamma(\cdot + c)\|_{L^2}^2 \,\mathrm{d}c \\
&= \frac{1}{2\pi L^2} \int_{\partial B_L(0)} \int_{\mathbb{R}^2} |\hat{\gamma}(k)(1 - e^{2\pi i c\cdot k})|^2 \,\mathrm{d}k \,\mathrm{d}c \\
&\geq \frac{1}{2\pi L^2} \int_{\{L|k|\geq 1\}} |\hat{\gamma}(k)|^2 \int_{\partial B_L(0)} |1 - e^{2\pi i c\cdot k}|^2 \,\mathrm{d}c \,\mathrm{d}k,
\end{aligned}$$

where the integral $\int_{\partial B_L(0)} |1 - e^{2\pi i c\cdot k}|^2 \,\mathrm{d}c$ is greater than L due to $L|k| \geq 1$ [15]. □

3.2 Proof of lower bound by contradiction

As a guidance, we may think of the construction from the previous section. Figure 3.1 shows a sketch of its major features and of what this implies for the Fourier transform of γ.

Before proceeding to the details, let us introduce some notation. Throughout this section, $\mathscr{O}$ denotes the optimal geometry and is understood to depend on ε without explicitly indicating this dependence. Likewise, the characteristic function χ of $\mathscr{O}$ and its variants such as γ, f_1, f_2 also depend on ε. We will use the small O notation $f(\varepsilon) = o(g(\varepsilon))$ to indicate $\frac{f(\varepsilon)}{g(\varepsilon)} \to_{\varepsilon\to 0} 0$. Furthermore, $\sim$ shall denote equality up to a constant factor independent of ε (but potentially depending on ℓ and F), and similarly, $\lesssim$, $\gtrsim$ shall denote less than or greater than up to a constant factor.

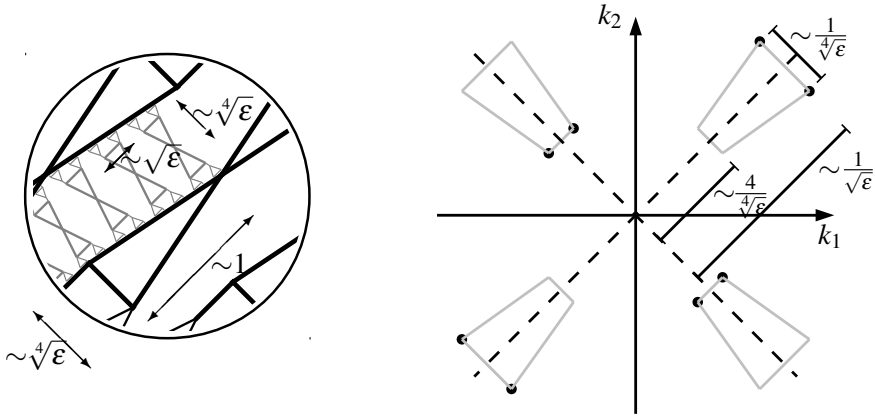

FIGURE 3.1. Left: Zoom into the optimal geometry from Figure 2.1. Right: Corresponding idealized sketch of the optimal geometry in Fourier space; the black dots are where we expect the major mass to be. The gray trapezoids indicate the regions outside which the support is shown to be negligible.

We shall prove the lower bound by contradiction; assume the excess energy to be $o(\sqrt{\varepsilon})$,

$$\mathrm{J}^{\varepsilon,F,\ell}[\mathscr{O}] - \mathrm{J}_0^{*,F,\ell} = \Delta\mathrm{J}^{F,\ell}_{\mathrm{elast}}(\mathscr{O}) + \varepsilon\mathrm{Per}(\mathscr{O}) = o(\sqrt{\varepsilon})\,. \tag{3.4}$$

A short sketch of the argument is as follows. Using the estimates from the previous section, we will first show that $\hat{f}_i$, $i = 1,2$, essentially lie within the wedges of Figure 3.1 (Proposition 3.7). From this and the fact $\hat{\chi} = \hat{\chi} * \hat{\chi}$ (which roughly means that $(\hat{f}_1 + \hat{f}_2)$ approximately equals $(\hat{f}_1 + \hat{f}_2) * (\hat{f}_1 + \hat{f}_2)$) we infer that $\hat{f}_1 * \hat{f}_2$ or equivalently $f_1 f_2$ has negligible L^2-norm (Lemma 3.9; for technical reasons, f_1 and f_2 are replaced here by approximations g_1 and g_2). Finally, based on f_1 and f_2 we decompose the domain Ω into the region where material struts are more or less aligned with v_1 and the region where struts are aligned with v_2. Using these domains in Lemma 3.3 and also the estimate that $f_1 f_2 \approx 0$ then finally yields a contradiction.

Specifying all volume fractions. Lemmas 3.1 and 3.2 now provide the L^2-mass of χ, f_1, and f_2.

Proposition 3.6 (Volume fractions)**.** *Under assumption* (3.4) *and for* $i = 1,2$ *we have*

$$\begin{aligned}
\theta &= 2|F| + o(\sqrt[4]{\varepsilon})\,,\\
\|\gamma\|_{L^2}^2 &= \ell 2|F|(1-2|F|) + o(\sqrt[4]{\varepsilon})\,,\\
\|f_i\|_{L^2}^2 &= \ell|F|(1-2|F|) + o(\sqrt[4]{\varepsilon})\,.
\end{aligned}$$

Proof. Lemma 3.1 yields the estimate

$$\Delta\mathrm{J}^{F,\ell}_{\mathrm{elast}}(\mathscr{O}) \geq \ell\tfrac{(2|F|-\theta)^2}{\theta} = \ell 2|F|(\tfrac{2|F|}{\theta} - 1)(1 - \tfrac{\theta}{2|F|})\,,$$

which can be solved for $\frac{2|F|}{\theta}$ to yield $\frac{2|F|}{\theta} = 1 + o(\sqrt[4]{\varepsilon})$ and thus the desired estimate for θ. The second estimate now is a direct consequence of $\|\gamma\|_{L^2}^2 = \ell\theta(1-\theta)$.

Likewise, the estimate from Lemma 3.2,

$$\Delta \mathrm{J}_{\mathrm{elast}}^{F,\ell}(\mathscr{O}) \geq \frac{4F^2}{\theta^2 \max(\|f_1\|_{L^2}^2, \|f_2\|_{L^2}^2)} \left(\|f_i\|_{L^2}^2 - \frac{\ell\theta(1-\theta)}{2} \right)^2$$

together with $\max(\|f_1\|_{L^2}^2, \|f_2\|_{L^2}^2) \leq \|\gamma\|_{L^2}^2 = \ell\theta(1-\theta) \sim 1$ and $\theta \sim 2|F|$ implies

$$\frac{\|f_i\|_{L^2}^2}{\ell} = \frac{\theta(1-\theta)}{2} + o(\sqrt[4]{\varepsilon}),$$

which produces the final estimate. □

Localizing the Fourier support of γ. We now use Lemmas 3.1, 3.4, and 3.5 to show that the Fourier support of f_1 and f_2 (and thus of γ) is restricted to the wedges shown in Figure 3.1 (right).

Proposition 3.7 (Fourier support of γ)**.** *Under assumption* (3.4) *and for $i = 1, 2$ we have*

$$\int_{\mathbb{R}^2 \setminus W_i} |\hat{f}_i|^2 \, \mathrm{d}k = o(1)$$

for the wedge

$$W_i = \left\{ k \in \mathbb{R}^2 : \operatorname{dist}(\bar{k}, \{\pm v_i\}) < \sqrt[4]{\varepsilon},\ |k| < \tfrac{1}{\sqrt{\varepsilon}},\ |k \cdot v_i| > \tfrac{4}{\sqrt[4]{\varepsilon}} \right\}.$$

Proof. The estimate from Lemma 3.1 together with Proposition 3.6 implies

$$\Delta \mathrm{J}_{\mathrm{elast}}^{F,\ell}(\mathscr{O}) \geq \tfrac{4F^2}{\theta^2} \int_{\mathbb{R}^2} |\hat{\gamma}|^2 \operatorname{dist}^2(\bar{k}, B) \, \mathrm{d}k \gtrsim \sum_{i=1,2} \int_{\{\operatorname{dist}(\bar{k}, \{\pm v_i\}) \geq \sqrt[4]{\varepsilon}\}} \sqrt{\varepsilon} |\hat{f}_i|^2 \, \mathrm{d}k$$

so that the L^2-mass of $\hat{f}_1$ and $\hat{f}_2$ outside a wedge of angle $\sqrt[4]{\varepsilon}$ around the preferred directions must be negligible. Also, Lemma 3.5 for the choice $L = \sqrt{\varepsilon}$ implies that the L^2-mass of $\hat{\gamma}$ and thus $\hat{f}_1$ and $\hat{f}_2$ beyond the frequency $1/\sqrt{\varepsilon}$ is negligible. Finally, $\hat{\gamma}$, $\hat{f}_1$, and $\hat{f}_2$ have negligible L^2-mass at frequencies with $|k|_1 = |k_1| + |k_2| < 4/\sqrt[4]{\varepsilon}$. Indeed, assume the opposite, i. e. $\int_{\{|k|_1 \leq \frac{4}{\sqrt[4]{\varepsilon}}\}} |\hat{f}_1|^2 \, \mathrm{d}k \gtrsim 1$, then the choice $b = \sqrt[4]{\varepsilon}/4$ in Lemma 3.4 yields $\Delta \mathrm{J}_{\mathrm{elast}}^{F,\ell}(\mathscr{O}) \gtrsim \frac{2F^2}{\theta^2} 1/[1 + 32\|\gamma\|_{L^2}^4/b^2] \sim \sqrt{\varepsilon}$, a contradiction. The analogous result holds for f_2. □

Note that each bound in the definition of W_i may actually be multiplied by an arbitrary constant, since only the asymptotic behavior for $\varepsilon \to 0$ is considered. The above choice, in particular the factor 4 in the last bound, will become clear in the proof of Lemma 3.9, where it leads to a disjoint Fourier support of a number of functions.

For later purposes it is convenient to replace $\hat{f}_1$ and $\hat{f}_2$ by approximations $\hat{g}_1$ and $\hat{g}_2$ whose support completely lies in W_1 and W_2, respectively. If chosen properly,

these functions enjoy useful boundedness properties as summarized in the subsequent proposition. For a compact notation, we also introduce the characteristic function of Ω,

$$X(x) = \begin{cases} 1 & \text{if } x \in \Omega, \\ 0 & \text{else,} \end{cases}$$

with $\hat{X}(k) = \ell e^{-2\pi i \frac{1}{2} k \cdot \binom{\ell}{1}} \operatorname{sinc}(k_1 \ell) \operatorname{sinc}(k_2)$.

Proposition 3.8 (Decomposition of γ)**.** *Under assumption* (3.4)*, there exist functions g_1, g_2, and g satisfying, for any $p \in (1,\infty)$ and a constant $C > 0$,*

$$\begin{gathered} \chi = \theta X + g_1 + g_2 + g, \\ \operatorname{supp} \hat{g}_i \subset W_i, \quad i = 1,2, \\ \|f_1 - g_1\|_{L^2}, \|f_2 - g_2\|_{L^2}, \|g\|_{L^2} = o(1), \\ \|g_1\|_{L^p}, \|g_2\|_{L^p}, \|g\|_{L^p} \le C. \end{gathered}$$

Proof. It is easy to see that the proof of Proposition 3.7 can be modified to show that $\hat{f}_1$ and $\hat{f}_2$ have negligible L^2-mass outside the wedges

$$\tilde{W}_i = \left\{ k \in \mathbb{R}^2 : \operatorname{dist}(\bar{k}, \{\pm v_i\}) < \tfrac{1}{4}\sqrt[4]{\varepsilon}, |k| < \tfrac{1}{2\sqrt{\varepsilon}}, |k \cdot v_i| > \tfrac{8}{\sqrt[4]{\varepsilon}} \right\}.$$

We will define $\hat{g}_1$ and $\hat{g}_2$ by restricting $\hat{f}_1$ and $\hat{f}_2$ to subsets of W_1 and W_2. In order to still have boundedness of the g_i in L^p, we will thus have to apply a multiplier theorem. To this end, for $i = 1,2$ and $m,n \in \mathbb{Z}$ consider the sets

$$\begin{aligned} Q_{m,n} &= \left((-2^{m+1}, -2^m] \cup [2^m, 2^{m+1})\right) \times \left((-2^{n+1}, -2^n] \cup [2^n, 2^{n+1})\right), \\ \tilde{Q}_{m,n} &= \tfrac{1}{\sqrt{2}} \left(\begin{smallmatrix} 1 & 1 \\ -1 & 1 \end{smallmatrix}\right) Q_{m,n}, \\ V_i &= \bigcup_{\tilde{Q}_{m,n} \cap \tilde{W}_i \neq 0} \tilde{Q}_{m,n}. \end{aligned}$$

We have $V_i \subset W_i$. Let us now define g_1, g_2, and g via

$$\hat{g}_i(k) = \begin{cases} \hat{f}_i(k) & \text{if } k \in V_i \\ 0 & \text{else} \end{cases}$$

and $\gamma = \chi - \theta X = g_1 + g_2 + g$. By the Marcinkiewicz Multiplier Theorem [12, Theorem 5.2.4], for any $p \in (1,\infty)$ we have

$$\|g_1\|_{L^p}, \|g_2\|_{L^p}, \|g\|_{L^p} \le C \max(p, \tfrac{1}{p-1})^{12} \|\gamma\|_{L^p} = C \max(p, \tfrac{1}{p-1})^{12} \sqrt[p]{(1-\theta)\theta^p + \theta(1-\theta)^p}$$

for a fixed $C > 0$ (note that the coordinate system has to be rotated by $\frac{\pi}{4}$ to apply [12, Theorem 5.2.4]). Furthermore, by definition, the L^2-norms of $f_1 - g_1$, $f_2 - g_2$, and g or equivalently the L^2-norms of their Fourier transforms are bounded above by $\|\hat{\gamma}\|_{L^2(\mathbb{R}^2 \setminus (\tilde{W}_1 \cup \tilde{W}_2))} = o(1)$. □

In the next paragraph we will try to obtain a more explicit characterization of the functions g_1 and g_2, using the fact that they essentially represent a decomposition of the characteristic function χ (or rather of γ).

Exploiting the properties of characteristic functions to characterize the decomposition of γ. Now we will exploit the fact that χ is a characteristic function, i. e. $\chi = \chi \cdot \chi$. By inserting $\chi = \theta X + g_1 + g_2 + g$ and comparing the supports of the different terms on either side of $\hat{\chi} = \hat{\chi} * \hat{\chi}$, we will see that $g_1 g_2$ is negligible, a fact which should be wrong intuitively: it is easily conceivable that non-negligible $\hat{g}_1$ and $\hat{g}_2$ with support as in Figure 3.1 will not produce negligible $\hat{g}_1 * \hat{g}_2$. This will ultimately lead to the desired contradiction.

Lemma 3.9 (Characterization of Fourier decomposition)**.** *Under assumption* (3.4) *and for g_1, g_2 from Proposition 3.8 we have*

$$\begin{aligned} \|g_1 g_2\|_{L^2} &= o(1)\,, \\ g_1^2 &= (1-2\theta) g_1 + \tfrac{\|g_1\|_{L^2}^2}{\ell} X + \xi_1\,, \\ g_2^2 &= (1-2\theta) g_2 + \tfrac{\|g_2\|_{L^2}^2}{\ell} X + \xi_2 \end{aligned}$$

for two functions ξ_1 and ξ_2 satisfying, with $i = 1, 2$,

$$\begin{aligned} \|\xi_1 + \xi_2\|_{L^2} &= o(1)\,, \\ \int_{\mathbb{R}^2} \xi_i \,\mathrm{d}x &= 0\,, \\ \int_{\{k\,:\,\max(|k\cdot v_1|, |k\cdot v_2|) \geq \frac{1}{\sqrt[4]{\varepsilon}}\}} |\hat{\xi}_i|^2 \,\mathrm{d}x &= o(1)\,. \end{aligned}$$

Proof. The relation $\hat{\chi} = \hat{\chi} * \hat{\chi}$ implies

$$\hat{\chi} = \hat{\chi} * \hat{\chi} = 2\hat{g} * \hat{\chi} - \hat{g} * \hat{g} + 2\theta \hat{X} * \hat{\chi} - \theta^2 \hat{X} * \hat{X} - 2\theta \hat{X} * \hat{g} + (\hat{g}_1 + \hat{g}_2) * (\hat{g}_1 + \hat{g}_2)\,.$$

Using $\hat{X} * \hat{X} = \hat{X}$, $\hat{X} * \hat{\chi} = \hat{\chi}$, $\|\hat{g} * \hat{\chi}\|_{L^2} = \|g\chi\|_{L^2} \leq \|g\|_{L^2}$, $\|\hat{g} * \hat{X}\|_{L^2} = \|gX\|_{L^2} \leq \|g\|_{L^2}$, and $\|\hat{g} * \hat{g}\|_{L^2} = \|g^2\|_{L^2} \leq \sqrt{\|g\|_{L^2} \|g\|_{L^6}^3} \lesssim \sqrt{\|g\|_{L^2}}$, we arrive at

$$(1-2\theta)\hat{\chi} + \theta^2 \hat{X} = \hat{g}_1 * \hat{g}_1 + \hat{g}_2 * \hat{g}_2 + 2\hat{g}_1 * \hat{g}_2 + \hat{r}$$

or equivalently

$$\theta(1-\theta)\hat{X} + (1-2\theta)(\hat{g}_1 + \hat{g}_2 + \hat{g}) = \hat{g}_1 * \hat{g}_1 + \hat{g}_2 * \hat{g}_2 + 2\hat{g}_1 * \hat{g}_2 + \hat{r}\,,$$

where the remainder $\hat{r}$ is $o(1)$ in L^2. The basic idea now is the following: All terms involving g or r can be neglected. Among the remaining terms in the equation, none intersects the support of $\hat{g}_1 * \hat{g}_2$, hence no term balances $\hat{g}_1 * \hat{g}_2$. This implies that $\hat{g}_1 * \hat{g}_2$ must also be negligible. Let us proceed to the details:

The supports of $\hat{g}_i$, $\hat{g}_j * \hat{g}_j$, and $\hat{g}_1 * \hat{g}_2$ do not intersect for $i \neq j$. In particular, $\operatorname{supp}(\hat{g}_1 * \hat{g}_2) \subset \{k : |k \cdot v_1|, |k \cdot v_2| \geq \frac{2}{\sqrt[4]{\varepsilon}}\}$ only intersects the support of $\hat{r}$, $\hat{g}$, and $\hat{X}$

so that the above equality implies

$$\|\hat g_1 * \hat g_2\|_{L^2}^2 \le \tfrac12 \int_{\{k:|k\cdot v_1|,|k\cdot v_2|\ge \frac{2}{\sqrt[4]{\varepsilon}}\}} |(1-2\theta)\hat g + \theta(1-\theta)\hat X - \hat r|^2 \,\mathrm{d}k = o(1)\,.$$

To better characterize $\hat g_1 * \hat g_1$ and $\hat g_2 * \hat g_2$, define the two residual functions ξ_1, ξ_2 via

$$\begin{aligned}\hat g_1 * \hat g_1 &= (1-2\theta)\hat g_1 + \tfrac{\|g_1\|_{L^2}^2}{\ell}\hat X + \hat\xi_1\,,\\ \hat g_2 * \hat g_2 &= (1-2\theta)\hat g_2 + \tfrac{\|g_2\|_{L^2}^2}{\ell}\hat X + \hat\xi_2\,.\end{aligned}$$

The residuals ξ_1, ξ_2 satisfy

$$\int_{\mathbb{R}^2} \xi_i \,\mathrm{d}x = \int_{\mathbb{R}^2} g_i^2 - (1-2\theta)g_i - \tfrac{\|g_i\|_{L^2}^2}{\ell} X \,\mathrm{d}x = -(1-2\theta)\int_{\mathbb{R}^2} g_i \,\mathrm{d}x = -(1-2\theta)\hat g_i(0) = 0\,,$$

$$\begin{aligned}\|\hat\xi_1 + \hat\xi_2\|_{L^2} &= \|\hat g_1 * \hat g_1 + \hat g_2 * \hat g_2 - (1-2\theta)(\hat g_1 + \hat g_2) - \tfrac{\|g_1\|_{L^2}^2 + \|g_2\|_{L^2}^2}{\ell}\hat X\|_{L^2}\\ &= \|(1-2\theta)\hat g - \hat r - 2\hat g_1 * \hat g_2 + (\theta(1-\theta) - \tfrac{\|\gamma - g\|_{L^2}^2}{\ell})\hat X\|_{L^2} = o(1)\end{aligned}$$

as well as

$$\int_{\{k:\max(|k\cdot v_1|,|k\cdot v_2|)\ge \frac{1}{\sqrt[4]{\varepsilon}}\}} |\hat\xi_i|^2 \,\mathrm{d}x = o(1)\,,$$

since in the region $\max(|k\cdot v_1|, |k\cdot v_2|) \ge \frac{1}{\sqrt[4]{\varepsilon}}$, the only terms with non-negligible L^2-mass are $\hat g_i * \hat g_i$ and $(1-2\theta)\hat g_i$, $i = 1,2$, so that in this region $\hat g_i * \hat g_i - (1-2\theta)\hat g_i = 0$ up to an L^2 negligible error. □

Remark 3.10. Note that the above information can be used to see that the L^4- and L^2-mass of g_1 and g_2 outside Ω are negligible. Indeed, for $i = 1,2$ we have

$$\begin{aligned}o(1) = \|g_1 g_2\|_{L^2(\mathbb{R}^2)}^2 &\ge \int_{\mathbb{R}^2\setminus\Omega} g_1^2 g_2^2 \,\mathrm{d}x = \int_{\mathbb{R}^2\setminus\Omega} g_i^2 (g_i^2 + 2g_i g + g^2)\,\mathrm{d}x\\ &= \|g_i\|_{L^4(\mathbb{R}^2\setminus\Omega)}^4 + \int_{\mathbb{R}^2\setminus\Omega} g_i^2(2g_i g + g^2)\,\mathrm{d}x \ge \|g_i\|_{L^4(\mathbb{R}^2\setminus\Omega)}^4 + 2\int_{\mathbb{R}^2\setminus\Omega} g_i^3 g\,\mathrm{d}x\,,\end{aligned}$$

where the integral is bounded in absolute value via Hölder's inequality by $2\|g\|_{L^2}\|g_i\|_{L^6}^3 \le C\|g\|_{L^2} = o(1)$, using Proposition 3.8. Also,

$$\|g_i\|_{L^2(\mathbb{R}^2\setminus\Omega)}^2 \le \|g_i\|_{L^4(\mathbb{R}^2\setminus\Omega)}\|g_i\|_{L^{\frac43}(\mathbb{R}^2\setminus\Omega)} = o(1)\,,$$

again using Proposition 3.8 for the $L^{\frac43}$-norm.

Deriving a contradicting spatial separation of g_1 and g_2. We would like to better understand ξ_1 and ξ_2. We first change g_1 and g_2 slightly to make $\|\hat{g}_1 * \hat{g}_2\|_{L^2}$ exactly zero. To this end, introduce the characteristic functions

$$\chi_{g_1}(x) = \begin{cases} 1 & \text{if } x \in \Omega \text{ and } |g_2(x)| < |g_1(x)|\,, \\ 0 & \text{else,} \end{cases} \qquad \chi_{g_2} = X - \chi_{g_1}\,.$$

Intuitively, χ_{g_1} indicates the region in which the struts are roughly aligned with v_2 and χ_{g_2} the region in which the struts are aligned with v_1. Now we can define

$$G_1 = \gamma\chi_{g_1}\,, \quad G_2 = \gamma\chi_{g_2}\,, \quad \Xi_1 = \xi_1 + g_1 - G_1\,, \quad \Xi_2 = \xi_2 + g_2 - G_2\,,$$

and we obtain the following characterizations.

Lemma 3.11 (Characterization of domain decomposition)**.** *Under assumption* (3.4)*, letting $\approx$ denote equality up to a remainder with L^2-norm of $o(1)$ we have, for $i = 1,2$,*

$$G_i \approx g_i\chi_{g_i} \approx g_i \approx g_i X \approx f_i$$

as well as

$$\begin{aligned} \chi &= G_1 + G_2 + \theta X\,, \\ G_1G_2 &= 0\,, \\ \Xi_i &\approx \xi_i\,, \\ \Xi_1 + \Xi_2 &\approx 0\,, \\ \chi_{g_i} &\approx \tfrac{1}{2}X - \tfrac{1}{\theta(1-\theta)}\Xi_i\,. \end{aligned}$$

Proof. $g_i \approx g_i X$ follows from Remark 3.10. Note that for $i = 1,2$ and $j \neq i$ we have

$$\|g_i\chi_{g_j}\|_{L^2}^2 \leq \int_{\{x\in\Omega\,:\,|g_i(x)|\leq|g_j(x)|\}} |g_i(x)|^2\,\mathrm{d}x \leq \int_\Omega |g_1g_2|\,\mathrm{d}x \leq \sqrt{\mathrm{Vol}(\Omega)}\|g_1g_2\|_{L^2} = o(1)$$

from Lemma 3.9. This directly implies

$$\|g_i - g_i\chi_{g_i}\|_{L^2} \leq \|g_i - Xg_i\|_{L^2} + \|Xg_i - g_i\chi_{g_i}\|_{L^2} = \|g_i - Xg_i\|_{L^2} + \|g_i\chi_{g_j}\|_{L^2} = o(1)\,,$$

from which we finally obtain

$$\|g_i - G_i\|_{L^2} \leq \|g_i - g_i\chi_{g_i}\|_{L^2} + \|g_j\chi_{g_i}\|_{L^2} + \|g\chi_{g_i}\|_{L^2} = o(1)$$

and thus $\Xi_i \approx \xi_i$ as well as $\Xi_1 + \Xi_2 \approx \xi_1 + \xi_2 \approx 0$ via Lemma 3.9.

The relations $\chi = G_1 + G_2 + \theta X$ and $G_1G_2 = 0$ follow directly from the definition of the G_i. This now implies $G_i(x) \in \{-\theta, 0, 1-\theta\}$ for almost all x as well as $\{x \in \mathbb{R}^2 : \chi_{g_i}(x) = 0\} = \{x \in \mathbb{R}^2 : G_i(x) = 0\}$ or equivalently $(G_i + \theta X)(x) \in \{0, \theta, 1\}$ with $\{x \in \mathbb{R}^2 : \chi_{g_i}(x) = 0\} = \{x \in \mathbb{R}^2 : (G_i + \theta X)(x) = \theta\}$. Thus, for

$j \neq i$,

$$\begin{aligned}\chi_{g_j} &= \tfrac{(G_i+\theta X)-(G_i+\theta X)^2}{\theta(1-\theta)} = X + \tfrac{G_i-G_i^2-2\theta G_i}{\theta(1-\theta)} \\ &= X + \tfrac{g_i+\xi_i-\Xi_i-G_i^2-2\theta G_i}{\theta(1-\theta)} = X + \tfrac{g_i^2+2\theta g_i-\|g_i\|_{L^2}^2 X/\ell-\Xi_i-G_i^2-2\theta G_i}{\theta(1-\theta)} \\ &= (1-\tfrac{\|g_i\|_{L^2}^2}{\ell\theta(1-\theta)})X - \tfrac{\Xi_i}{\theta(1-\theta)} + \tfrac{2\theta(g_i-G_i)+g_i^2-G_i^2}{\theta(1-\theta)} \approx \tfrac{1}{2}X - \tfrac{\Xi_i}{\theta(1-\theta)}\,,\end{aligned}$$

using $\|G_i - g_i\|_{L^2} = o(1)$, $\|g_i\|_{L^2}^2 = \|f_i\|_{L^2}^2 + o(1) = \frac{\ell\theta(1-\theta)}{2} + o(1)$, and $\|G_i^2 - g_i^2\|_{L^2}^2 = \int_{\mathbb{R}^2} |G_i - g_i|^2 |G_i + g_i|^2 \,\mathrm{d}x \leq \|G_i - g_i\|_{L^2} \|G_i - g_i\|_{L^6} \|G_i + g_i\|_{L^6}^2$ (where G_i is bounded and g_i is bounded in L^6 by Proposition 3.8). □

The previous lemma shows that Ξ_1 and Ξ_2 or equivalently ξ_1 and ξ_2 are intimately connected with the characteristic functions χ_{g_1} and χ_{g_2}. Recall that $\hat{\xi}_1$ and $\hat{\xi}_2$ are supported at frequencies smaller than $1/\sqrt[4]{\varepsilon}$. In other words, the predominant length scales of ξ_1 and ξ_2 and thus of χ_{g_1} and χ_{g_2} are larger than $\sqrt[4]{\varepsilon}$, which itself is the largest significant length scale occuring in χ. This would mean that the regions with struts supporting stress in direction v_1 and struts supporting stress in direction v_2 are spatially separated, which cannot be optimal. To quantify the suboptimality, we now finally apply Lemma 3.3 for the two regions indicated by χ_{g_1} and χ_{g_2}. To this end, let $\gamma_i = \tilde{\gamma}_i - X \fint_\Omega \tilde{\gamma}_i \,\mathrm{d}x$ for $\tilde{\gamma}_i = (\chi-1)\chi_{g_i} = G_i - (1-\theta)\chi_{g_i}$ (recall $\chi(x) = 0$ and $\chi_{g_i}(x) = 1 \Leftrightarrow G_i(x) = -\theta$) and observe

$$\begin{aligned}\gamma_i &= G_i - (1-\theta)\chi_{g_i} - \tfrac{\int_\Omega G_i - (1-\theta)\chi_{g_i}\,\mathrm{d}x}{\mathrm{Vol}(\Omega)} X \approx g_i - (1-\theta)\chi_{g_i} - \tfrac{\int_\Omega g_i - (1-\theta)(\frac{X}{2} - \frac{\Xi_i}{\theta(1-\theta)})\,\mathrm{d}x}{\mathrm{Vol}(\Omega)} X \\ &= g_i - (1-\theta)(\chi_{g_i} - \tfrac{X}{2}) - \tfrac{\int_\Omega \frac{\xi_i + (g_i - G_i)}{\theta}\,\mathrm{d}x}{\mathrm{Vol}(\Omega)} X \approx g_i + (1-\theta)(\tfrac{X}{2} - \chi_{g_i}) \approx g_i + \tfrac{\Xi_i}{\theta}\,,\end{aligned}$$

where $\approx$ stands for equality up to a function with L^2-norm of $o(1)$. Inserting this relation in Lemma 3.3 now yields

$$\begin{aligned}&\Delta \mathrm{J}_{\mathrm{elast}}^{F,\ell}(\mathscr{O}) \geq \ell 4F^2(\tfrac{1}{\theta} - 1)(1-2\alpha) \\ &- \tfrac{4F^2}{\theta^2} \int_{\mathbb{R}^2} \left| \overline{\hat{g}_1 \bar{k}^\perp} \cdot \left(\begin{smallmatrix} \alpha & 1-\alpha \\ 1-\alpha & \alpha \end{smallmatrix}\right) \bar{k}^\perp + \overline{\hat{g}_2 \bar{k}^\perp} \cdot \left(\begin{smallmatrix} -\alpha & 1-\alpha \\ 1-\alpha & -\alpha \end{smallmatrix}\right) \bar{k}^\perp + (1-\theta)\alpha \overline{(\hat{\chi}_{g_2} - \hat{\chi}_{g_1})} \right|^2 \mathrm{d}k + o(1)\,.\end{aligned}$$

Note that $\|\hat{\chi}_{g_1} - \hat{\chi}_{g_2}\|_{L^2}^2 = \|\chi_{g_1} - \chi_{g_2}\|_{L^2}^2 = \ell$ and furthermore that $\hat{g}_1$, $\hat{g}_2$, and

$$\hat{\chi}_{g_2} - \hat{\chi}_{g_1} \approx \frac{\Xi_1 - \Xi_2}{\theta(1-\theta)} \approx \frac{\xi_1 - \xi_2}{\theta(1-\theta)}$$

all have different support (up to an L^2-negligible overlap, see the definition of g_i and Lemma 3.9). Hence, assuming $0 \le \alpha \le \frac{1}{3}$, we obtain

$$\begin{aligned}
\Delta \mathrm{J}^{F,\ell}_{\mathrm{elast}}(\mathscr{O}) &\ge \ell 4F^2(\tfrac{1}{\theta}-1)(1-2\alpha)\\
&\quad - \tfrac{4F^2}{\theta^2}\int_{\mathbb{R}^2} |\hat g_1|^2(\bar k^\perp \cdot \left(\begin{smallmatrix} \alpha & 1-\alpha \\ 1-\alpha & \alpha\end{smallmatrix}\right)\bar k^\perp)^2 + |\hat g_2|^2(\bar k^\perp \cdot \left(\begin{smallmatrix} -\alpha & 1-\alpha \\ 1-\alpha & -\alpha\end{smallmatrix}\right)\bar k^\perp)^2 \,\mathrm{d}k\\
&\quad - \tfrac{4F^2}{\theta^2}(1-\theta)^2\alpha^2\|\hat\chi_{g_2}-\hat\chi_{g_1}\|^2_{L^2} + o(1)\\
&\ge \ell 4F^2(\tfrac{1}{\theta}-1)(1-2\alpha) - \tfrac{4F^2}{\theta^2}\int_{\mathbb{R}^2} |\hat f_1|^2(1-2\alpha)^2 + |\hat f_2|^2(1-2\alpha)^2\,\mathrm{d}k\\
&\quad - \tfrac{4F^2}{\theta^2}\ell(1-\theta)^2\alpha^2 + o(1)\\
&= \ell\frac{4F^2}{\theta^2}\left[\theta(1-\theta)[(1-2\alpha)-(1-2\alpha)^2] - (1-\theta)^2\alpha^2\right] + o(1)\\
&\sim \ell F^2(1-2|F|)
\end{aligned}$$

after maximizing over $0 \le \alpha \le \frac{1}{3}$ (note that for $\alpha = 0$ the square bracket is zero with positive derivative of order one). This yields the desired contradiction so that we must have $\mathrm{J}^{\varepsilon,F,\ell}[\mathscr{O}] - \mathrm{J}_0^{*,F,\ell} \gtrsim \sqrt{\varepsilon}$ as $\varepsilon \to 0$.

So far we have shown that for fixed F and ℓ there are an $\varepsilon_0 > 0$ and a constant $C > 0$ such that $\min_{\mathscr{O}\subset\Omega} \mathrm{J}^{\varepsilon,F,\ell}[\mathscr{O}] - \mathrm{J}_0^{*,F,\ell} \ge C\sqrt{\varepsilon}$ for all $\varepsilon < \varepsilon_0$. However, $\min_{\mathscr{O}\subset\Omega} \mathrm{J}^{\varepsilon,F,\ell}[\mathscr{O}] - \mathrm{J}_0^{*,F,\ell}$ is monotonously increasing in ε so that $\min_{\mathscr{O}\subset\Omega} \mathrm{J}^{\varepsilon,F,\ell}[\mathscr{O}] - \mathrm{J}_0^{*,F,\ell} \ge C\sqrt{\varepsilon_0}$ for all $\varepsilon \ge \varepsilon_0$. Combining both inequalities we arrive at the desired result, $\min_{\mathscr{O}\subset\Omega} \mathrm{J}^{\varepsilon,F,\ell}[\mathscr{O}] - \mathrm{J}_0^{*,F,\ell} \ge C\sqrt{\varepsilon_0/|F|}\sqrt{\varepsilon}$ for all $\varepsilon \le |F|$.

Appendix: Compliance associated with diffusing a uniaxial stress

Here we provide a detailed compliance estimate for a boundary layer in which the impact of a localized load diffuses over a larger material area. This estimate is merely needed for the refined construction in Remark 2.4, which allows to weaken the conditions on how small ε has to be relative to F for the upper bound on the energy scaling to hold. The load situation occurring in Remark 2.4 is of the type as in Figure A.1, right, where a thick material layer is under a uniform stress parallel to the layer (horizontal in Figure A.1) and is additionally loaded on either side (here top and bottom) with a stress normal to the layer and localized along a small segment of length d. The fact that the normal stress is applied locally, instead of evenly distributed over the whole width, results in an excess compliance (the compliance for the given d minus that for the case $d = w$), which is the quantity needed in Remark 2.4. Now the excess compliance in Figure A.1, right, is bounded above by twice the excess compliance in Figure A.1, center right, which again can be reduced to the excess compliance in Figure A.1, left, via Corollary A.2. The compliance in Figure A.1, left, is estimated in Proposition A.1.

Consider a rectangular piece of material with side lengths w and $\frac{w}{2}$, respectively, loaded as shown in Figure A.1, left. As mentioned above, this load geometry may

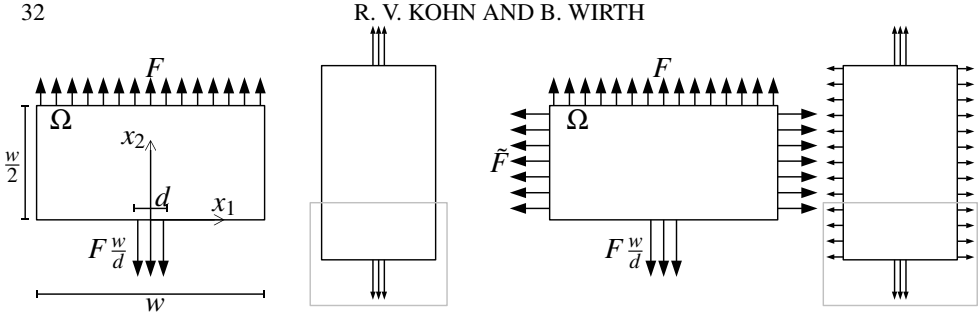

FIGURE A.1. The load geometry considered in Proposition A.1 (left) can be interpreted as a segment of a larger rectangular geometry over which the tensile stress diffuses (center left). The same holds for the load geometry from Corollary A.2 (center right and right).

be thought of as a segment of a larger rectangular domain at both sides of which a tensile stress is applied in a small region of width d (Figure A.1, center left). The tensile stress then diffuses over the whole width of the rectangle. Let Σ_{ad} denote the set of admissible stresses, i. e. those symmetric tensor fields which are divergence-free and satisfy the given boundary conditions.

Proposition A.1 (Compliance of stress diffusion)**.** *The compliance* $\min_{\sigma\in\Sigma_{\mathrm{ad}}}\int_\Omega|\sigma|^2\,\mathrm{d}x$ *of the configuration in Figure A.1, left, is bounded above by* $\frac{w^2F^2}{2}(1+\frac{\pi}{2}\ln\frac{w}{d})$.

Proof. It suffices to provide an admissible stress field σ or, via the identification $\sigma=\begin{pmatrix}\partial_{22}\phi & -\partial_{12}\phi\\ -\partial_{21}\phi & \partial_{11}\phi\end{pmatrix}$, a corresponding Airy stress function ϕ. Note that for $d=w$, the equilibrium stress is described by the Airy stress function

$$\phi^w(x_1,x_2)=F\tfrac{x_1^2}{2}\,.$$

Similarly, an Airy stress function describing a uniform tensile stress within a vertical strip of width $d<w$ is given by

$$\tilde\phi(x_1,x_2)=\begin{cases}F\frac{w}{d}\frac{x_1^2}{2} & \text{if } |x_1|\le\frac{d}{2}\,,\\ \frac{Fw}{2}(|x_1|-\frac{d}{4}) & \text{else.}\end{cases}$$

Now an Airy stress function admissible for the load configuration in Figure A.1 left can be constructed (abbreviating $r=\sqrt{x_1^2+x_2^2}$) as

$$\phi^d(x_1,x_2)=\phi^w(x_1,x_2)+\begin{cases}\tilde\phi(r,0)-\phi^w(r,0) & \text{if } r\le\frac{w}{2}\,,\\ \tilde\phi(\frac{w}{2},0)-\phi^w(\frac{w}{2},0) & \text{else.}\end{cases}$$

This yields the stress field

$$\sigma^d(x_1,x_2)=\left(\begin{smallmatrix}0&0\\0&F\end{smallmatrix}\right)+\begin{cases}F(\frac{w}{d}-1)I & \text{if } r\le\frac{d}{2}\,,\\ -FI+\frac{Fw}{2r}(I-e_r^\perp\otimes e_r^\perp) & \text{if } \frac{d}{2}\le r\le\frac{w}{2}\,,\\ 0 & \text{else,}\end{cases}$$

with $e_r^\perp = (-\sin\varphi, \cos\varphi)$, where $(x_1, x_2) = (r\cos\varphi, r\sin\varphi)$. We can thus bound the compliance above by

$$\begin{aligned}\int_{x_1=-\frac{w}{2}}^{\frac{w}{2}} \int_{x_2=0}^{\frac{w}{2}} |\sigma^d|^2 \,\mathrm{d}x_2\mathrm{d}x_1 &= \tfrac{\pi}{2}(\tfrac{d}{2})^2 F^2 \big((\tfrac{w}{d}-1)^2 + (\tfrac{w}{d})^2\big) + \big(\tfrac{w^2}{2} - \tfrac{\pi}{2}(\tfrac{w}{2})^2\big)F^2 \\ &\quad + \int_{r=\frac{d}{2}}^{\frac{w}{2}} \int_{\varphi=0}^{\pi} \left| \begin{pmatrix} -F + \frac{Fw}{2r}(1-\sin^2\varphi) & \frac{Fw}{2r}\sin\varphi\cos\varphi \\ \frac{Fw}{2r}\sin\varphi\cos\varphi & \frac{Fw}{2r}(1-\cos^2\varphi) \end{pmatrix} \right|^2 r\,\mathrm{d}\varphi\mathrm{d}r \\ &= \tfrac{\pi}{2}(\tfrac{d}{2})^2 F^2 \big((\tfrac{w}{d}-1)^2 + (\tfrac{w}{d})^2\big) + \big(\tfrac{w^2}{2} - \tfrac{\pi}{2}(\tfrac{w}{2})^2\big)F^2 \\ &\quad + \int_{r=d/2}^{w/2} \int_{\varphi=0}^{\pi} \Big[(\tfrac{Fw}{2r})^2 + F^2 - \tfrac{F^2 w}{r}\cos^2\varphi \Big] r\,\mathrm{d}\varphi\mathrm{d}r \\ &= \tfrac{w^2F^2}{2}(1 + \tfrac{\pi}{2}\ln\tfrac{w}{d}).\end{aligned}$$

□

The previous proposition says that if the load at the bottom is concentrated in a region of width d, then the excess compliance over the situation of a uniform stress distribution (i. e. $d = w$) is bounded by $\frac{\pi}{4}w^2F^2\ln\frac{w}{d}$. This stays true even if an additional horizontal load is applied on the left and right boundary as in Figure A.1 right.

Corollary A.2. *The compliance* $\min_{\sigma\in\Sigma_{\mathrm{ad}}} \int_\Omega |\sigma|^2\,\mathrm{d}x$ *of the configuration in Figure A.1, right, is bounded above by* $\frac{w^2}{2}(\tilde{F}^2 + F^2 + F^2\frac{\pi}{2}\ln\frac{w}{d})$.

Proof. We decompose the equilibrium stress field according to $\tilde{\sigma} + \sigma$ with $\tilde{\sigma} = \left(\begin{smallmatrix} \tilde{F} & 0 \\ 0 & 0 \end{smallmatrix}\right)$ so that σ must be the equilibrium stress field for the configuration from Proposition A.1. Now the compliance is given by

$$\int_\Omega |\tilde{\sigma} + \sigma|^2\,\mathrm{d}x = \int_\Omega |\tilde{\sigma}|^2\,\mathrm{d}x + \int_\Omega |\sigma|^2\,\mathrm{d}x + 2\int_\Omega \mathrm{tr}(\sigma^T\tilde{\sigma})\,\mathrm{d}x.$$

The first term is $\frac{w^2}{2}\tilde{F}^2$, the second is bounded by Proposition A.1, and the third is zero since σ satisfies

$$\begin{aligned} \textstyle\int_{-w/2}^{w/2} \sigma(x_1, x_2)\left(\begin{smallmatrix}0\\1\end{smallmatrix}\right)\mathrm{d}x_1 &= \left(\begin{smallmatrix}0\\Fw\end{smallmatrix}\right) && \forall x_2 \in [0, \tfrac{w}{2}], \\ \textstyle\int_0^{w/2} \sigma(x_1, x_2)\left(\begin{smallmatrix}1\\0\end{smallmatrix}\right)\mathrm{d}x_2 &= \left(\begin{smallmatrix}0\\0\end{smallmatrix}\right) && \forall x_1 \in [-\tfrac{w}{2}, \tfrac{w}{2}] \end{aligned}$$

so that $\int_\Omega \sigma\,\mathrm{d}x = \mathrm{Vol}(\Omega)\left(\begin{smallmatrix}0&0\\0&F\end{smallmatrix}\right)$. □

Acknowledgment.

RVK gratefully acknowledges support from NSF through grants DMS-0807347 and OISE-0967140. BW gratefully acknowledges the support of a Courant Instructorship during which this work was conducted.

Bibliography

[1] Allaire, G. *Shape optimization by the homogenization method*, *Applied Mathematical Sciences*, vol. 146, Springer-Verlag, New York, 2002.

[2] Allaire, G.; Aubry, S. On optimal microstructures for a plane shape optimization problem. *Structural Optimization* **17** (1999), 86–94.

[3] Allaire, G.; Jouve, F.; Toader, A.-M. Structural optimization using sensitivity analysis and a level-set method. *Journal of Computational Physics* **194** (2004), 363–393.

[4] Allaire, G.; Kohn, R. V. Optimal design for minimum weight and compliance in plane stress using extremal microstructures. *European J. Mech. A Solids* **12** (1993), no. 6, 839–878.

[5] Ambrosio, L.; Buttazzo, G. An optimal design problem with perimeter penalization. *Calculus of Variations and Partial Differential Equations* **1** (1993), no. 1, 55–69.

[6] Bendsøe, M. P.; Sigmund, O. *Topology optimization: theory, methods and applications*, Springer-Verlag, Berlin, 2003.

[7] Bourdin, B.; Chambolle, A. Design-dependent loads in topology optimization. *ESAIM Control Optim. Calc. Var.* **9** (2003), 19–48.

[8] Chambolle, A. A density result in two-dimensional linearized elasticity, and applications. *Archive for Rational Mechanics and Analysis* **167** (2003), no. 3, 211–233.

[9] Chan, A.; Conti, S. Energy scaling and branched microstructures in a model for shape-memory alloys with SO(2) invariance. *arXiv:1403.6242* (2014).

[10] Choksi, R.; Conti, S.; Kohn, R. V.; Otto, F. Ground state energy scaling laws during the onset and destruction of the intermediate state in a type I superconductor. *Comm. Pure Appl. Math.* **61** (2008), no. 5, 595–626. Available at: `http://dx.doi.org/10.1002/cpa.20206`

[11] Choksi, R.; Kohn, R. V.; Otto, F. Domain branching in uniaxial ferromagnets: a scaling law for the minimum energy. *Comm. Math. Phys.* **201** (1999), no. 1, 61–79. Available at: `http://dx.doi.org/10.1007/s002200050549`

[12] Grafakos, L. *Classical Fourier analysis*, *Graduate Texts in Mathematics*, vol. 249, Springer, New York, 2008, 2nd ed.

[13] Haber, R.; Jog, C.; Bendsøe, M. P. A new approach to variable-topology shape design using a constraint on perimeter. *Structural Optimization* **11** (1996), no. 1-2, 1–12.

[14] Hashin, Z.; Shtrikman, S. A variational approach to the theory of the elastic behaviour of multiphase materials. *J. Mech. Phys. Solids* **11** (1963), 127–140.

[15] Knüpfer, H.; Kohn, R. V.; Otto, F. Nucleation barriers for the cubic-to-tetragonal phase transformation. *Comm. Pure Appl. Math.* **66** (2013), no. 6, 867–904.

[16] Kohn, R.; Wirth, B. Optimal microstructures in compliance minimization for a uniaxial load. *Preprint* (2014).

[17] Kohn, R. V.; Müller, S. Surface energy and microstructure in coherent phase transitions. *Comm. Pure Appl. Math.* **47** (1994), no. 4, 405–435. Available at: `http://dx.doi.org/10.1002/cpa.3160470402`

[18] Kohn, R. V.; Strang, G. Optimal design and relaxation of variational problems. I. *Comm. Pure Appl. Math.* **39** (1986), no. 1, 113–137. Available at: `http://dx.doi.org/10.1002/cpa.3160390107`

[19] Kohn, R. V.; Strang, G. Optimal design and relaxation of variational problems. II. *Comm. Pure Appl. Math.* **39** (1986), no. 2, 139–182. Available at: `http://dx.doi.org/10.1002/cpa.3160390202`

[20] Kohn, R. V.; Strang, G. Optimal design and relaxation of variational problems. III. *Comm. Pure Appl. Math.* **39** (1986), no. 3, 353–377. Available at: `http://dx.doi.org/10.1002/cpa.3160390305`

[21] Penzler, P.; Rumpf, M.; Wirth, B. A phase-field model for compliance shape optimization in nonlinear elasticity. *ESAIM: Control, Optimisation and Calculus of Variations* **18** (2012), no. 1, 229–258.

[22] Strang, G.; Kohn, R. V. Optimal design in elasticity and plasticity. *International Journal for Numerical Methods in Engineering* **22** (1986), no. 1, 183–188. Available at: `http://dx.doi.org/10.1002/nme.1620220113`

[23] Zhou, S.; Wang, M. Y. Multimaterial structural topology optimization with a generalized Cahn–Hilliard model of multiphase transition. *Structural and Multidisciplinary Optimization* **33** (2007), 89–111.

Received Month 200X.